DESIGN AND SCALE-UP OF A NOVEL BIOMIMETIC MIXING SYSTEM FOR A CLOSED BIOREACTOR

by

Jayden Ryan Garfield

A thesis submitted to the faculty of
The University of Utah
in partial fulfillment of the requirements for the degree of

Master of Science

Department of Bioengineering

The University of Utah

May 2013

The University of Utah Graduate School

STATEMENT OF THESIS APPROVAL

The following faculty members served as the supervisory committee chair and members for the thesis of Jayden Ryan Garfield.

Dates at right indicate the members' approval of the thesis.

Robert W. Hitchcock, Chair	3/14/13	Date Approved
Kelly W. Broadhead, Member	3/14/13	Date Approved
Tomasz J. Petelenz, Member	3/14/13	Date Approved

The thesis has also been approved by Patrick A. Tresco

Chair of the Department/School/College of Bioengineering

and by Donna M. White, Interim Dean of The Graduate School.

ABSTRACT

The technologies and processes used in large scale cell bioprocessing, namely the impeller based stirred suspension bioreactor, were designed for the growth of robust and often immortal cell lines to produce protein based therapeutics. The turbulent fluid environment created by such systems was not designed to accommodate the delicate nature of stem cell suspension culture – in particular, to maintain the low shear stress and homogeneity required to retain an undamaged cell and unaltered phenotype. While new bioreactor designs have been developed to address the unique environmental needs of stem cell cultures, industrial volume scale-up is still unavailable.

In this work, a novel biomimetic mixing mechanism utilizing a silicone diaphragm and an alternating actuation mechanism has been designed and developed to produce adequate fluid mixing while maintaining a low shear stress environment. The unique design, characterized on a bench-top scale, has been scaled-up over a range of volumes from 100 – 3000 ml. Using particle image velocimetry, the fluid dynamics created by the novel mixing mechanism were qualitatively and quantitatively analyzed.

The mixing mechanism produced adequate fluid mixing within the vessel while maintaining mean shear stress levels more than 100 times lower than seen in impeller based spinner flasks. Furthermore, the mixing profile and mean shear stress levels

remained well below requirement levels ($\leq 0.3 \frac{\text{dynes}}{\text{cm}^2}$) regardless of reactor volume. In conclusion, we have developed a novel mixing system which overcomes shear stress limitations of current stirred suspension reactors in volumes ranging from 100-3000 ml.

TABLE OF CONTENTS

LIST OF TABLES

ACKNOWLEDGEMENTS

I would like to thank and acknowledge the mentoring and collaborative effort of Monir Parikh throughout the course of my research. I would also like to thank the members of my committee for the support and guidance both related and unrelated to my academic pursuits. I would like to thank my parents for giving me support, ambition, and work ethic. Finally, I thank my loving wife, Chloe, for her immeasurable love, support and encouragement.

I would like to acknowledge the funding for this project provided by Refine Technology.

CHAPTER 1

INTRODUCTION

Bioprocess Industry Background

In the late 20th century the biopharmaceutical industry transformed modern medicine with the large scale manufacture and use of protein therapeutics produced by engineered mammalian cells to treat a wide range of diseases [1]. Today, nearly 70% of all recombinant protein therapeutics are produced through robust Chinese hamster ovary (CHO) cells, with annual sales exceeding $30 billion worldwide for CHO cell-derived products alone [2]. CHO cells are the preferred production vehicle for a number of key reasons: robustness, ease of use, production track record, and most importantly, their suspension scalability to volumes in excess of 20000 liters in industrial bioreactors [3].

CHO cells are routinely cultured in bioreactors, which are devices in which biological or biochemical processes occur under closely monitored and tightly controlled conditions including homogeneity, mass transfer, pH, temperature, and oxygen concentration [4].

Two common bioreactor platforms currently exist: static and suspension reactors. Static bioreactor systems (t-flasks) are open systems where the culture chamber and its surroundings must be opened during inoculation, medium exchange, and harvesting. These processes increase contamination potential [5]. Furthermore, due

to the planar nature of static systems, mixing and concentration gradient limitations arise. Conversely, suspension bioreactors used in the production of molecular therapeutics are operated under well mixed closed conditions, which ensure a high quality, reproducible product.

The stirred tank bioreactor is the predominate bioreactor from bench-scale through large scale production due to its simplicity, performance, and industry experience [6], [7]. While stirred vessels are the industrial gold standard, there are other suspension culture systems such as cell culture bags, hollow fiber cartridges, fluidized or packed-beds, bubble-column or air-lift vessels, rotary cell culture systems, and microfluidic devices; each with their specific advantages and disadvantages [8].

Cells are typically grown on 100 – 300 μm microcarriers in large scale suspension bioreactors in order to maximize surface to volume area [9], [10]. In such cases, the bioreactor mixing mechanism must utilize very low agitation intensities because the microcarrier is on the same order of magnitude as the eddy sizes in highly turbulent flow environments [11] and therefore more susceptible to hydrodynamic damage than single cells in suspension.

Bioreactor Mixing Functionality

Mixing is a critical component of any stirred tank bioreactor. Insufficient mixing leads to settling and inhomogeneous environmental zones due to limited mass transfer. Inadequately mixed commercial culture systems with significant dissolved CO_2 concentration gradients lead to drastic pH differences between fluid parcels within the chamber [6], [10], [12]. Inadequate mixing using impellers also results in dissolved O_2

gradients, which have a great effect on the cellular metabolism and final product's quality [11], [13]. A case-by-case solution to this challenge has typically been developed as the bioreactor volume process is scaled up, resulting in numerous impeller configurations [6].

All impellers are designed to homogenously mix cells, gases, and nutrients throughout the bioreactor vessel. This action evenly disperses oxygen and nutrients required for healthy growth, discourages settling, and maintains a uniform culture temperature [14]. In stirred bioreactors, this agitation causes energy transfer from the impeller to the culture medium, resulting in areas of intense turbulence and localized shear stresses on particles in the reactor. This occurs regardless of suspension methodology: single cells in suspension, cells attached to microcarriers, or the surface of cell aggregates [15]. The sensitivity of mammalian cells to shear forces (from shear induced cellular response [11] to lysis) has led to an extensive effort to vary and optimize the impeller mixing system to find the balance between sufficient mass transfer and hydrodynamic damage induced by the sweeping impeller blades.

Environmental Effects on CHO Cells

The major processing stress common to all mammalian cell culture is hydrodynamic shear stress, whether in stirred tank reactors or during manual cell culture operations. Three mechanisms of potential damage to cells have been reported: collisions between cells or microcarriers with other beads, collisions with parts of the reactor (impeller and probes), and interactions with turbulent eddies the size of the cell or microcarrier [16]. Fluid associated shear stress can result in cell death, cell apoptosis,

and nonlethal physiological responses [11]. Nonlethal responses can be found in the range of 1 – 10 Pa (10-100 $\frac{dynes}{cm^2}$) and can alter cell function, affect proliferation and viability, alter metabolism, and affect the surface content of cellular receptors of CHO cells [11]. Optimized impeller designs have led to stirred bioreactors within the safe shear stress tolerance range for robust mammalian cells [14].

Stem Cell Therapy

As protein therapy did 20 years ago, stem cells are poised to revolutionize modern medicine due to their regenerative potential and multilineage differentiation capacity. Stem cell therapies may well form the basis of future healthcare with applications in regenerative medicine, tissue engineering, and drug screening. Prochymal®, developed by Osiris Therapeutics, is a mesenchymal stem cell (MSC) therapeutic used to treat acute graft-versus-host disease in children which gained Canadian health regulators' approval in early 2012 making it the first stem cell drug to be approved for a systemic disease anywhere in the world [17]. Industrial and academic innovators are concurrently investigating the use of stem cells for the treatment of multiple diseases including neurodegenerative disorders [18], cardiac disease [19], diabetes [20], spinal cord injury [21], and amyotrophic lateral sclerosis [22].

Successful implementation of stem cell therapies will require a system capable of producing both the *quality* and *quantity* of cells required for widespread therapeutic benefit at an affordable cost. The number of cells utilized in cell therapy applications falls in the range of tens of millions to billions of cells per patient, per treatment [23].

For example, following myocardial infarction approximately $1x10^9$- $2x10^9$ cells are required to replace damaged cardiac tissue [19], [24]. For the treatment of diabetes, successful islet transplantation requires approximately 9000 islets per kilogram body weight [25] or $1.3x10^9$ insulin producing β-cells per 70-kg patient [20]. A bioartificial liver device comprising of only 10-20% of the number of native cells contains approximately 10^{10} hepatocytes and can support a patient with severe hepatic failure [26]. These examples suggest that 1 – 2 billion cells per patient is a useful benchmark to estimate production requirements in industrial stem cell bioprocess development, which would require 1-3 liters of suspended cell culture [27]. In addition, it is important to highlight that while molecular therapeutics are harvested as cell products, the stem cell itself is the product for stem cell therapies.

Cell Sources

Mesenchymal stem cells (MSC) are an attractive adult stem cell source because of their ease of access, isolation, and extensive expansion capability [28], [29]. Additionally, MSCs can be preserved and stored with minimal loss in potency [30]. These stem cells are also capable of multilineage differentiation [31], can exert an immunosuppressive effect *in vitro* and *in vivo* by acting on all immune effectors [32], and exhibit trophic effects mediated by the wide range of growth factors and cytokines they produce [33]. Finally, owning to their lack of a major histocompatibility complex, human trials of MSCs have shown no adverse reactions to allogeneic versus autologous transplants, which makes these cells ideal candidates for large scale expansion for stem

cell therapies [34], [35]. MSCs have shown great capacity for clinical applications in cardiovascular [36], neurological [37], and musculoskeletal disorders [38].

While MSCs have shown great potential for use in clinical settings, they are found in very low numbers in human tissue. The frequency in human bone marrow has been estimated to be on the order of 0.001 – 0.01% of total nucleated cells. In addition, the frequency declines with age, from 1 per 10^4 in a newborn to approximately ½ per 10^6 nucleated marrow cells in an 80 year old individual [39]. Therefore, large scale *in vitro* expansion, 30+ fold, is required in order to reach the quantity of cells required for clinical application.

Environmental Sensitivity of MSCs

Stem cells respond to various environmental cues *in vitro* in order to proliferate, maintain potency, or regulate differentiation. These cues can include biochemical factors, cell-cell interactions, cell-matrix interactions, and mechanical stimuli [40], [41], [42]. Dissolved O_2 concentration plays an important role in the regulation of MSC proliferation and differentiation [43][44]. Culture pH also has a considerable effect on the metabolic activity of cells and is carefully regulated *in vivo* by complex mechanisms influenced by carbon dioxide, lactate production and many elements of serum. Growth and differentiation of stem cells is also strongly dependent on pH [45]. The effects of hydrodynamic fluid shear stresses and strains have also been linked to the induction of physical, biochemical, and epigenetic cellular responses, all of which directly affect MSCs ability to proliferate, maintain potency, or differentiate [40], [42].

There is growing evidence that MSC proliferation and differentiation, such as osteogenic differentiation, are both sensitive to hydrodynamic fluid shear stress [46]. In three-dimensional MSC seeded constructs, an average surface shear stress of $5x10^{-5}$ Pa ($0.0005 \frac{dynes}{cm^2}$) corresponded to increased proliferation and cell viability, whereas higher shear stresses of $1x10^{-3}$ Pa ($0.01 \frac{dynes}{cm^2}$) resulted in the upregulation of mRNA expression of a variety of osteoblastic proteins leading to expression of alkaline phosphatase activity and increased calcium deposition [47]. Thus, *in vitro*, these microenvironmental conditions must be carefully replicated, monitored and maintained.

MSC Expansion

While the molecular therapy industry has optimized the large scale manufacture of recombinant proteins using mammalian cells in large-scale bioreactor vessels, the field of stem cell therapy is still in its infant stages. Traditionally, culturing stem cells has been performed on flat, two-dimensional surfaces such as tissue culture flasks and well-plates to produce pure populations of undifferentiated cells. This is due to the t-flask's simplicity, low cost, and ease of handling. Based on the benchmark quantity requirements of 1 – 2 billion cells per patient defined above, multiple two-dimensional parallel plates are recently being used as a means of large scale cell manufacture for clinical applications. Current multiple parallel plates can provide the cell numbers required for clinical trial testing and limited commercialization. A 40 layer vessel has a large surface area available for growth which can be manipulated by several robotic systems and drive the lot size to 30 – 100 billion cells / lot [48].

Although they are easy to use, static cultures such as 2D t-flasks have industrial scale limitations including concentration gradient development, lack of online control of environmental conditions, and limited surface areas to volume ratios [24]. Stirred bioreactors, which are successfully used in the molecular therapeutics industry due to their large scale production capabilities, are now being examined for the expansion of stem cells. These stirred bioreactors provide high surface area to volume ratios and a more tightly controlled environment for growth, which may be critical for successful MSC cultivation as seen by their sensitivity to environmental conditions [42], [49]. Several groups have reported success in expanding MSCs on microcarriers and in suspension in stirred vessels while retaining differentiation potential [50], [51], [52].

In order to circumvent the high shear environment imparted by impeller based stirred suspension cultures, NASA develop a rotating-wall vessel (RWV) optimized to produce laminar flow and minimize the mechanical shear and turbulence on cell aggregates in culture [53]. The RWV is composed of a horizontally rotating cylindrical culture vessel with a coaxial tubular oxygenator. This bioreactor is thought to largely solve the challenges of suspension culture – suspending cells and microcarriers without inducing large degrees of shear and turbulence while providing adequate nutrition and oxygenation [54]. Although RWV provides efficient gas transfer and low shear environment for cell growth, they are limited in scalability to a working volume of 500 ml and therefore may not be suitable for large scale expansion of allogeneic therapies [55].

Thus, as evident from the history and current industry standards, the bioprocess techniques and methodologies widely used in protein therapy have been applied to the

infant industry of stem cell therapy. However, it is important to again highlight that while molecular therapeutics are harvested as cell products, the stem cell itself is the product for stem cell therapies. The industry standard stirred bioreactor vessel was not designed to address the delicate and unique requirements of stem cells. Existing designs which fulfill these requirements, such as the RWV, face serious scalability challenges which may invalidate them as industrial volume candidates. Table 1.1 shows the advantages and disadvantages of select bioreactor systems. A novel bioreactor mixing mechanism with low shear is needed to deliver both the *quality* and *quantity* of cells required by the regenerative medicine and tissue engineering applications of the near future.

Design and Development

The initial design goal of this research project was to create a proof of concept mixing system which challenges and seeks to shift current gold standard means of suspension culture through the use of a novel mixing diaphragm based upon proven legacy technology and designed using a requirements based approach that will result in mixing process with subthreshold shear.

Legacy Technology

Refine Technology's patented Alternating Tangential Flow (ATF™ System) has revolutionized the biopharmaceutical industry and recently took second place in the "Technology of the Decade" awards presented by Bioprocess International [56]. The ATF™ System is based upon the technology of alternating tangential flow, created by

the action of a diaphragm moving upwards and downwards within a pump head, connected to filter housing and attached to a standard bioreactor, Figure 1.1. Applications of this system include: concentrated fed-batch, high productivity continuous culture, virus production and filtration, rapid media removal and exchange, clarification and harvest, cell and product concentration, microcarrier wash, perfusion, diafiltration, medium exchange and cell separation. The interest in the system as the legacy technology is due to the linear scalability from benchtop to manufacturing that is possible with such a simple technology. The large surface area of the diaphragm minimizes shear and supports extremely high cell concentrations. It is hypothesized that a novel mixing mechanism based upon ATF™ technology would overcome limitations with stirred suspension bioreactors associated with ex vivo expansion of MSCs.

Design Requirements

The bioreactor design requirements will need to address the metabolic and environmental needs of the MSC cells including availability of nutrients and removal of waste products, appropriate cell attachment conditions, hydrodynamic conditions, and a clear harvesting and storage protocol. The first leg in achieving the next generation of bioreactors tailored for MSC expansion is the focus of this thesis. The work presented here was to identify an appropriate design which featured a mixing mechanism that would produce homogenizing low shear stresses ($< 0.3 \frac{dynes}{cm^2}$) through radial mixing without negatively impacting media mixing and distribution. This is in stark contrast to the rotational or radial mixing of standard impeller approaches used in current

bioreactors where shear stresses are orders of magnitude higher (gold standard approach). Development of the low shear stress mixing mechanism would be the first step in achieving the design requirements needed to allow Refine Technology to challenge the current clinical practice of stem cell expansion and thereby set the stage for industrial scale regenerative medicine and tissue engineering applications.

Biomimetic Innovation

John O. Dabiri *et al.* at the Biological Propulsion Laboratory of California Institute of Technology have extensively studied the dynamic locomotion mechanisms of aquatic organisms, namely jellyfish [57]. Their studies encompass the transport of fluid mass, momentum and general fluid dynamics generated through the swimming motions of jellyfish [58]. Of particular interest is the concept of optimal vortex formation during jellyfish motion. Multiple studies have evaluated the influence of the vortex ring formation and vortical mixing on the environmental fluid [59], [60]. The locomotive motion of jellyfish has been found to be highly efficient and even a significant contributor to ocean mixing [61].

In this work, it is hypothesized that incorporating the general geometric relations of jellyfish in a diaphragmatic mixing mechanism will produce sufficient mixing in an efficient, low shear manner. These geometric considerations include the bell shape and aspect ratio, membrane thickness, and the length and spacing of the fins. These characteristics will be included in the geometric design of the diaphragm. Furthermore, notable functional design elements for the biomimetic device derived from the jellyfish swimming analysis are (1) alternating up and down motions, (2) motionless delays at

the end of both the upstroke and downstroke, (3) radial symmetry, and (4) flexible hinges/fins that are free to undergo flapping deformations due to the cyclic motion within the fluid [62].

Scalability

A review of the bioreactor technologies reveals the need for a design which uniquely fulfills fluid dynamic requirements including homogenous mixing and low shear stress [55]. However, of equal importance is the capacity for scalability [7]. Current challenges in developing a system capable of clinical production volumes include: (1) limited ability to scale-up or down, and (2) mixing profiles that are predictable, controllable, and reproducible throughout scale-up to production volumes [55], [5], [63]. For a design solution to gain traction as a viable alternative to stirred vessel systems, it must be scalable to production volumes comparable to those of stirred reactors [6].

The requirements based design approach identified requirements from four main areas: (1) stem cell needs, (2) legacy technology, (3) jellyfish biomimicry, and (4) clinical/industrial need for scalability. A summary of these requirements is provided in Table 1.2.

Table 1.1 Comparison of Select Existing Bioreactors

Bioreactor System	Advantages	Disadvantages
T-Flask	Simple	Difficult Scale-Up
	Low Cost	Labor Intensive
		Lack of Online-Monitoring
		De-differentiation
		Low Surface Area : Volume Ratio
Cell Factories	Larger Scale (relative to T-Flask)	Difficult Scale-Up
		Labor Intensive
		De-differentiation
		Low Surface Area : Volume Ratio
Rotating-Wall Bioreactor	Low Shear	Difficult Scale-Up
	Homogenous Environment	Unpredictable Mixing
		High Cost
Wave Bioreactor	Low Shear	Difficult Scale-Up
		Unpredictable Mixing
		High Cost
Stirred Suspension Bioreactor	High Surface Area : Volume Ratio	High shear forces
	Easily Scalable	Inhomogeneous Mixing Environments
	Extensive Knowledge/Experience	

Table 1.2 Design Input Requirements

Source	Requirement
Stem Cell Need	Reduced turbulent hydrodynamic environment through minimized or eliminated small eddy formation.
	Large rotational flows which predictably and adequately distribute fluid movement
	Homogenous low shear stresses ($< 0.3 \frac{dynes}{cm^2}$)
Legacy Technology	Alternating up and down motions
	Direct contact with culture media
Jellyfish Biomimicry	Alternating up and down motions
	Motionless delays at the end of the upstroke and downstroke
	Radial symmetry
	Flexible hinges/fins that are free to undergo flapping deformation due to the cyclic motion within the fluid
Clinical/Industrial Need	Scalable design

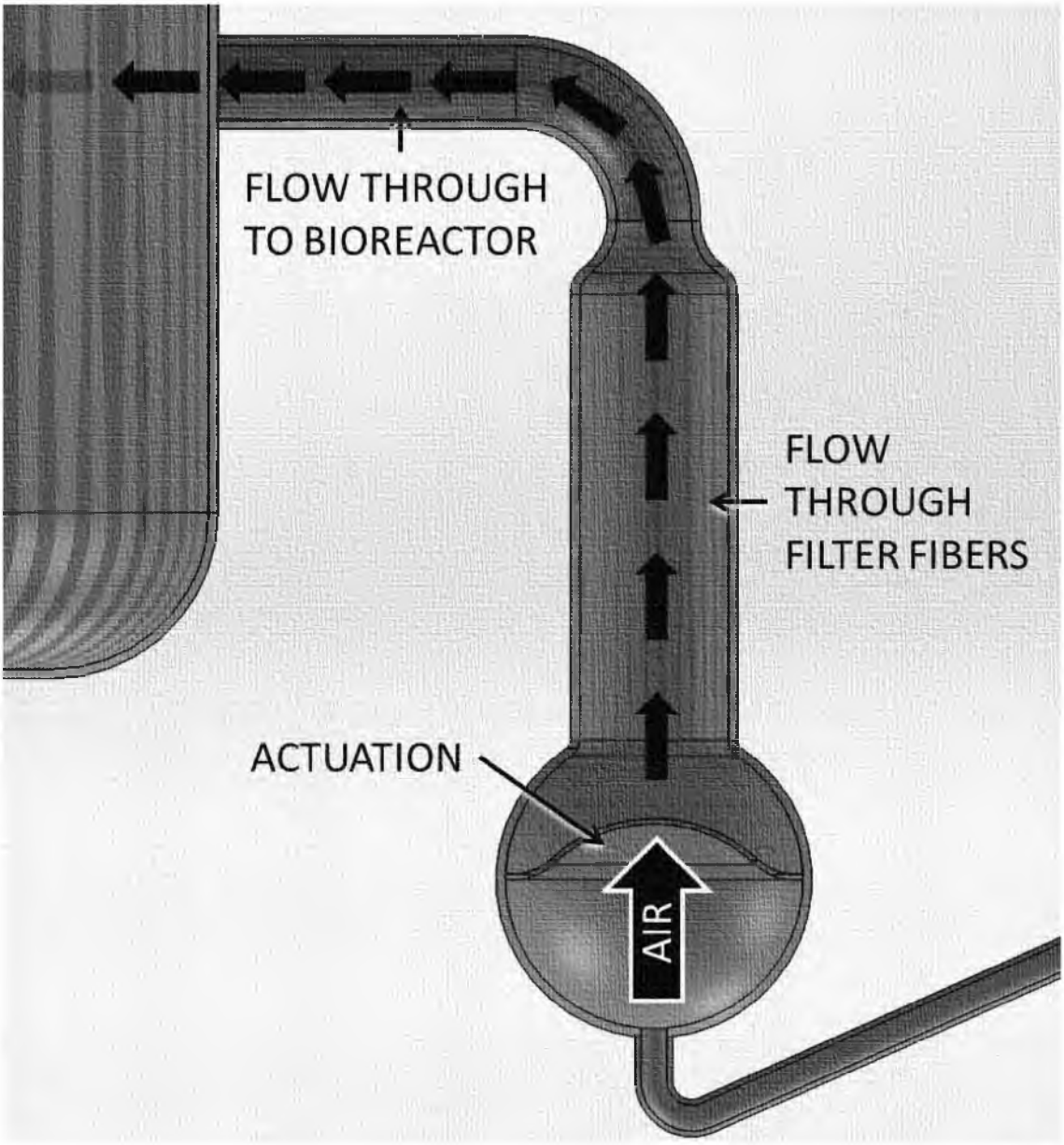

Figure 1.1 The Alternating Tangential Flow (ATF™) system is used as a perfusion accessory for existing bioreactors. The system utilizes a spherically housed silicone diaphragm, which is pneumatically actuated in alternating up and downstrokes. This displaces the adjacent fluid through the filter fibers.

CHAPTER 2

METHODS

Bioreactor Design

A final design was selected to meet the requirements derived from the legacy ATF™ technology, biomimetic model, proof of concept prototypes, and the delicate nature of MSCs as design input as seen in Figure 2.1. The proposed system consists of an inverted jellyfish-like diaphragm that is mechanically actuated up and down. The diaphragm is fixed in the bottom of the reactor vessel and is in direct contact with the culture media.

Mixing Mechanism Operation

A silicone diaphragm is affixed to the bottom surface of a curved bioreactor vessel. The deformation of the diaphragm results in a displacement of the culture media in alternating directions, thus promoting fluid mixing within the reactor chamber. Furthermore, the diaphragm design incorporates biomimetic elements such as radial symmetry and flexible hinges/fins. These elements result in the formation of both starting and stopping vortex rings, which has been shown to greatly influence localized fluid dynamics. The silicone diaphragm has an interfacing sleeve which elastically fits over a linear actuator (Model 43H4A-2.33-815, Haydon Kerk Motion Solutions, Hollis,

USA) coupler aligned concentrically with the diaphragm and vessel; see the system schematic in Figure 2.1. Precise control of stroke length, stroke speed, and delay between upstrokes and downstrokes is implemented using a custom control program that was designed using LabView (USB-6211 National Instruments, Austin, USA) and a microstep driver (Gecko, Energy Micro, Oslo, Norway).

Prototype Fabrication

The selected design was modeled using SolidWorks 3D software (SolidWorks Corporation, Waltham, USA). The 3D models were converted to g-code computer-aided manufacturing files using both CamBam and MecSoft Corporation's Visual Mill software. The curved reactor bottom geometry was machined using CNC milling from stock cast acrylic and then polished to clear surfaces, see Figure 2.2. The machined acrylic reactor base was then fused to a 2.5 inch (63.5mm) clear cast acrylic tube using methylene chloride. Additionally, molds for the silicone diaphragm were printed using an Alaris 30 (Objet, Eden Prairie, USA) rapid prototyping printer. The silicone diaphragm was cast in the custom molds using a 1:10 ratio of VST50 (Factor II Inc., Lakeside, USA) silicone to catalyst. A mounting base to house the linear actuator was precision milled from polyurethane foam board. Each upstroke and downstroke of the mixing diaphragm had a stroke rate of 13.49 mm/sec with a stroke length of 17.4625 mm. The cycle is delayed with a 3 second pause following both the upstroke and downstroke. The system design parameters utilized in the prototype are seen in Table 2.1.

Particle Image Velocimetry

Particle image velocimetry (PIV) is used to visualize particle motion within a fluid flow. It is used as a quantitative tool that can verify that the proposed system achieves the design goals of mixing with concomitant low shear. As demonstrated by Sucosky *et al.* particle-imaging velocimetry utilizes optical techniques and statistical analyses to determine the instantaneous velocity fields within a fluid on a given reference plane [64]. This technique has been extensively characterized and optimized by groups such as Adrian, 1991 [65]; Willert and Gharib, 199l [66]; and Wetserweel, 1997 [67].

In this work, we used PIV analysis to determine the velocity magnitudes, shear stresses, vortex locations, and streamlines within the mixing fluid. The basic schematic for the PIV analysis employed is seen in Figure 2.3. The flow is tracked by optically reflective/fluorescent particles that are suspended within the fluid. A planar laser is projected through the medium and creates a reference plane of reflective particles. A Vision Research high speed camera (Phantom MIRO eX4) tracks the position of these particles at a rate of 50 frames per second. A given particle is "tracked" between adjacent frames by comparing the position of a given particle at two adjacent frames. Then using the frame right and displacement distance, a calculation can determine the instantaneous velocity of that particle. Correlation for all points in a frame results in a velocity gradient tensor which describes the change of velocity throughout the flow, as seen in Equation 2.1. Further computational analyses of these velocity fields yield multiple fluid dynamic parameters, such as dilation and shear stresses (Equation 2.2) and vorticity or rotation (Equation 2.3), of any fluid parcel at a given point.

$$\frac{du_i}{dx_j} = \frac{1}{2}\left(\frac{du_i}{dx_j} + \frac{du_j}{dx_i}\right) + \frac{1}{2}\left(\frac{du_i}{dx_j} - \frac{du_j}{dx_i}\right) = e_{ij} + r_{ij} \qquad \textbf{Equation 2.1}$$

$$e_{ij} = \frac{1}{2}\left(\frac{du_i}{dx_j} + \frac{du_j}{dx_i}\right) \qquad \textbf{Equation 2.2}$$

$$\mathbf{r_{ij} = -\frac{1}{2}\varepsilon_{ijk}\omega_k = \frac{1}{2}\left(\frac{du_i}{dx_j} - \frac{du_j}{dx_i}\right)} \qquad \textbf{Equation 2.3}$$

In Equation 2.1, $\frac{du_i}{dx_j}$ represents the index notation velocity component *du* in a given axial direction (*i, j, k*) with relation to each standard orthogonal axis (*i, j, k*). The resultant is a 3x3 matrix of the three-dimensional velocity (m/s) for every fluid parcel in the evaluated space. This velocity gradient tensor can be further defined as the combination of both the deviatoric element e_{ij} (Equation 2.2) and the rotational element r_{ij} (Equation 2.3). The symmetric term of the velocity gradient, $\frac{du_i}{dx_j}$, is the strain rate tensor, e_{ij}. The diagonal of the strain rate tensor encodes the compression or expansion of a fluid element, while the off-diagonal elements represent the shear rate of the fluid element. The antisymmetric component of the velocity gradient tensor represents the rigid rotation of the fluid element with angular velocity ω.

Prototype Bioreactor Particle Image Velocimetry

Figure 2.4 shows a custom stabilization and alignment fixture that was constructed to ensure repeatable planar illumination and recording across multiple trials. The fixture included an adjustable mounting bracket for the green laser module (Beam of Light Technologies, Clackamas, USA) as well as an adjustable mounting base for the

high speed camera. The Vision Research high speed camera was placed on the mounting base and focused on the center plane of the reactor vessel. The prototype bioreactor was filled with 150 mL of distilled water seeded with 212-250 μm fluorescent beads (Cospheric, Santa Barbara, USA) at a density of 2.5 mg/ml wet with a surfactant, TWEEN 80 (Sigma Aldrich, St. Louis, USA), prior to use. The system was run for a short time until a steady state flow was visually confirmed in the vessel. The flow was then captured at a rate of 50 frames per second for roughly 25 seconds of continuous cyclic actuation of the biomimetic ATF diaphragm mixing mechanism. The captured video was processed using an open-source image processing package (FIJI) into an image stack with sequential image slices representing a 20 ms time delay [68].

Barrel Distortion Correction

Successful and credible results from particle image velocimetry rely on the accurate location of any given particle within the analysis field. The captured light reflected from the fluorescent beads must pass through three mediums: distilled water, acrylic, and air. Refraction occurs as the light passes from one medium to another at the interface plane according to Snell's Law (Equation 2.4).

$$\frac{\sin(\theta_1)}{\sin(\theta_2)} = \frac{n_2}{n_1} \qquad \textbf{Equation 2.4}$$

Each θ is the angle of entry in relation to the normal of the interface plane and each *n* is the refractive index of each material that the light passes through. As the light

passes through the curved surfaces of a cylinder, barrel distortion, or magnification of the fluid within the cylinder, is seen.

A calibration fixture was designed and constructed which consists of a calibration plate, aligned brackets, and a removable acrylic cylinder of the same dimensions as the prototype bioreactor vessel as seen in Figure 2.5A. The calibration plate was dimensioned at 63.5 mm wide to tightly fit inside of the acrylic cylinder. The plate was coated with an opaque black aerosol paint and a 0.3 mm hole pattern was precisely cut at 3.175 mm vertical and horizontal spacing as seen in Figure 2.5B.

To correct for the refraction that occurs in the captured images, an elastic transformation algorithm (BUnwarpJ) was applied to return the images to their true locations within the vessel [69]. A schematic of this process flow is shown in Figure 2.6. First, the calibration fixture was immobilized in relation to the camera using the alignment fixture. The camera was focused on the calibration plate plane, which was directly aligned with the central plane of bioreactor vessel when mounted. A light source was placed behind the calibration plate to illuminate the hole pattern and improve image contrast. An image of the calibration plate in open air was recorded. Next, the removable cylinder was placed over the calibration plate and the inner space was filled with distilled water, causing barrel distortion due to the refraction through the water and acrylic cylinder. This distorted image was recorded and the resulting data files were loaded into FIJI and the plug-in BUnwarpJ with the water distorted image as the 'source' and the unaltered air image as the 'target'.

BUnwarpJ allows correlates landmarks between two images and computes the transformation required to match the source image to the target image. The illuminated

holes in the calibration plate were matched as the correlated landmarks on each image. The image registration settings of BUnwarpJ were input per the values in Table 2.2. The registration was run and an elastic transform file was obtained. This tranform file was then applied to every image slice from the captured actuation video using a custom scripted macro through the FIJI plug-in interface.

Correction Validation Method

To validate the correct transformation a second calibration plate was constructed with letter sequences replacing the hole patterns. The same process depicted in Figure 2.6 was followed with hole pattern transformation field being applied to the distorted letter sequence image. This transformation outputted a corrected letter sequence image. This corrected image was then quantitatively compared to an open air image of the letter sequence to determine the accuracy of the horizontal correction. The corrected image can be qualitatively compared to both the raw distorted image and the open air image in Figure 2.8. The quantitative comparison can be seen in Figure 2.9. There was a difference in the horizontal measurement of 2.6 ± 0.71 mm, or a 97.7% ± 0.63% match of the corrected image to the open air image. It was observed that a small region directly adjacent to the inner vessel wall on either side of the image was blurred by the transformation.

Data Analysis

After correction for barrel distortion, the image stack was loaded into MATLAB (Mathworks) using PIVlab, an open source "Time-Resolved Digital Particle Image

Velocimetry Tool for MATLAB" [70]. A region of interest containing the flow was selected. All default image preprocessing was deactivated. The PIV algorithm was set to conduct three interrogation passes for particle correlation. Pass 1 area was set at 100 px with an overlap step of 50%, Pass 2 area at 90 px with 50% step, and Pass 3 area at 80 px and 50% step. Once the correlation between temporally adjacent images was complete, the software was spatially calibrated. The open air calibration plate image was loaded into PIVlab and the real distance of 3.175 mm was assigned to adjacent holes in the image. The time step between image slices of 20 ms was also entered. This calibration resulted in equivalent software values of 1 px = 0.11mm and 1px/frame = 5.48 mm/s.

A single actuation cycle consists of (1) a downstroke, (2) a 3 second delay, (3) an upstroke, and (4) a 3 second delay preceding the downstroke of the next cycle. Three distinct actuation cycles were independently analyzed. From the calibrated image stack, PIVlab derived the following steady-state mean values: streamlines, velocity magnitude, vorticity, vortex location, and shear rate. The maximum and minimum values of each parameter for the steady-state mean were also recorded. Shear stress is defined as the dynamic viscosity (0.01002 $\frac{dynes*s}{cm^2}$ for water at 20°C) multiplied with the shear rate ($\frac{1}{s}$). Statistical analysis consisting of calculating the mean and standard deviation of distinct actuation cycles was utilized wherever applicable.

Mixing System Scale-Up

To understand the scalability of the novel biomimetic ATF™ mixing mechanism, three vessel sizes were fabricated to represent industrial relevant volumes: 125 ml, 500 ml, and 1000 ml, shown in Figure 2.9. For ease of nomenclature, the three vessels were referred to as 125V, 500V, and 1000V. The dimensions of each reactor size are listed in Table 2.3. The 125V and 500V reactor sizes utilized the original biomimetic silicone diaphragm. The 1000V reactor used a scaled up silicone diaphragm that was 1.5 times bigger in select dimensions while all other parameters are held constant, see Figure 2.10. This scaling factor is the same as the increase of the inner diameter between the 500V and 1000V sizes. Finally, actuation parameters such as stroke rate and delay remained unchanged while stroke length was increased to account for the larger diaphragm (Table 2.3).

To better characterize the performance and scalability of the novel mixing mechanism, each reactor size (125V, 500V, 1000V) was evaluated at different working volumes ranging from 100 – 3000 ml. Refer to Table 2.4 for the list of volumes for each respective reactor size. Three distinct actuation cycles were analyzed for each volume.

Low shear homogenous mixing was evaluated by a comparison of the derived streamlines, velocity magnitudes, vortex location, and shear rates. The maximum and minimum values of each parameter for the steady-state mean of each working volume were recorded and analyzed.

Table 2.1 Prototype Bioreactor Parameters

Parameter	Material/Value
Biomimetic ATF diaphragm	Silicone, Shore A 30
Motor housing	Polyurethane
Reactor vessel material	Acrylic
Vessel inner diameter	63.5 mm
Vessel height	144.8 mm
Working fluid	Distilled water
Fluid density	$1\ \frac{g}{cm^2}$
Fluid volume	150 mL
Fluid dynamic viscosity	$0.01002\ \frac{dynes*s}{cm^2}$
Stroke length	17.46 mm
Stroke rate	$13.49\ \frac{mm}{s}$
Delay duration	3 seconds

Table 2.2 BUnwarpJ Registration Settings

Parameter	Setting
Initial Deformation	Fine
Final Deformation	Super Fine
Divergence Weight	0.0
Curl Weight	0.0
Landmark Weight	50.0
Image Weight	0.1
Consistency Weight	10.0
Stop Threshold	0.01

Table 2.3 Scaled Reactor Parameters

Reactor Size	Inner Diameter		Height		Stroke Length		Stroke Rate	
	in.	cm	in.	cm	in.	mm	in./s	mm/s
125V	2.50	6.35	5.7	14.48	0.6875	17.463	0.5313	13.49
500V	3.75	9.52	8.0	20.32	0.6875	17.463	0.5313	13.49
1000V	5.75	14.60	9.65	24.51	1.40625	35.72	0.5313	13.49

Table 2.4 Tested Reactor Volumes

125V (ml)	500V (ml)	1000V (ml)
100	300	1000
150	400	1250
200	500	1500
250	600	1750
300	700	2000
	800	2500
	900	3000
	1000	

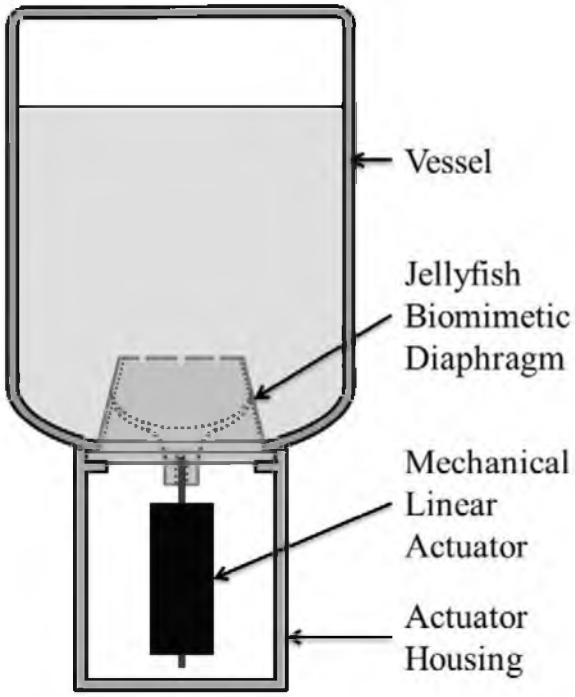

Figure 2.1 The novel biomimetic mixing bioreactor system consists of four key elements: (1) the culture vessel which contains the fluid medium, (2) the jellyfish biomimetic silicone diaphragm which is mechanically coupled to the (3) linear actuator fixed inside the (4) actuator housing.

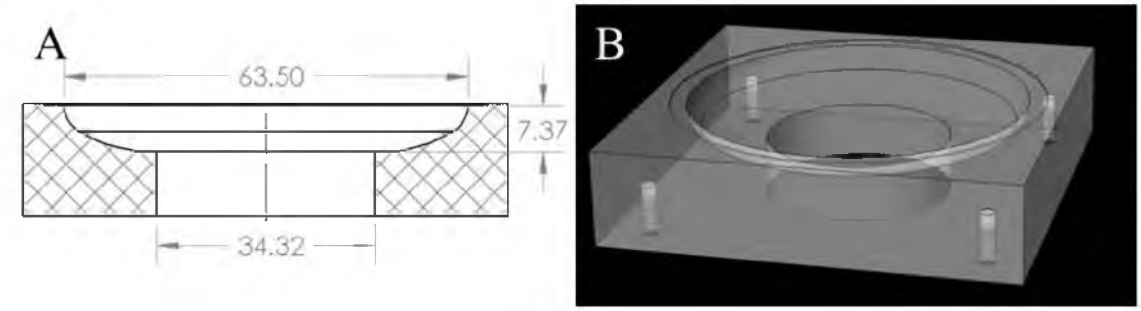

Figure 2.2 Curved reactor vessel bottom showing (A) cross-section dimensions (mm) and (B) perspective views.

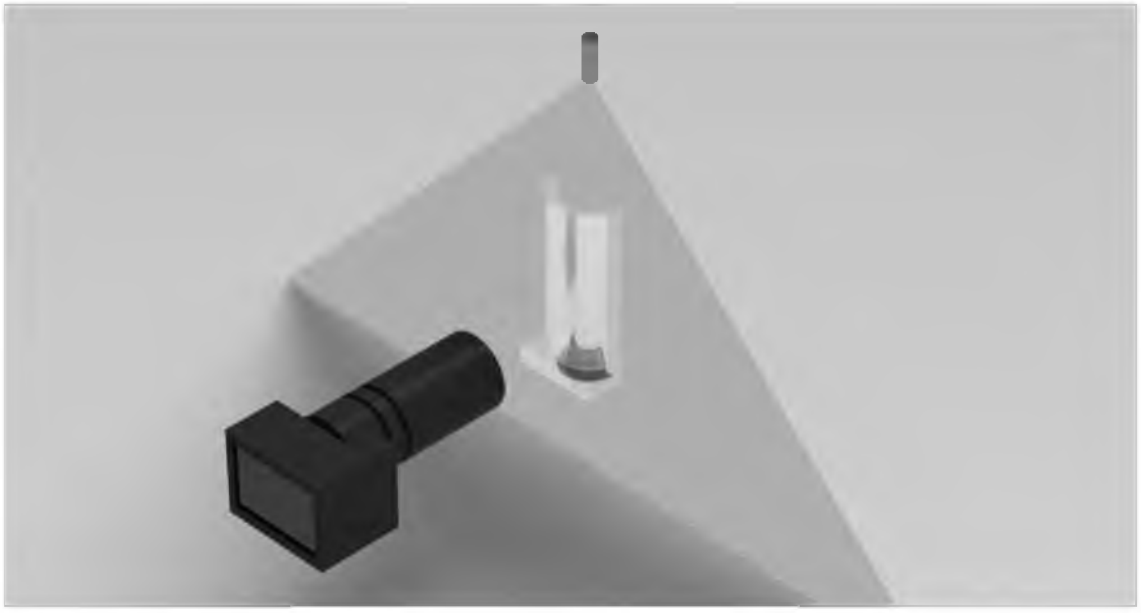

Figure 2.3 The basic schematic for particle image velocimetry (PIV). PIV analysis utilizes correlation software and a high speed camera to visualize the fluid flow by tracking fluorescent particles suspended within the fluid. The suspended particles are illuminated with a planar laser.

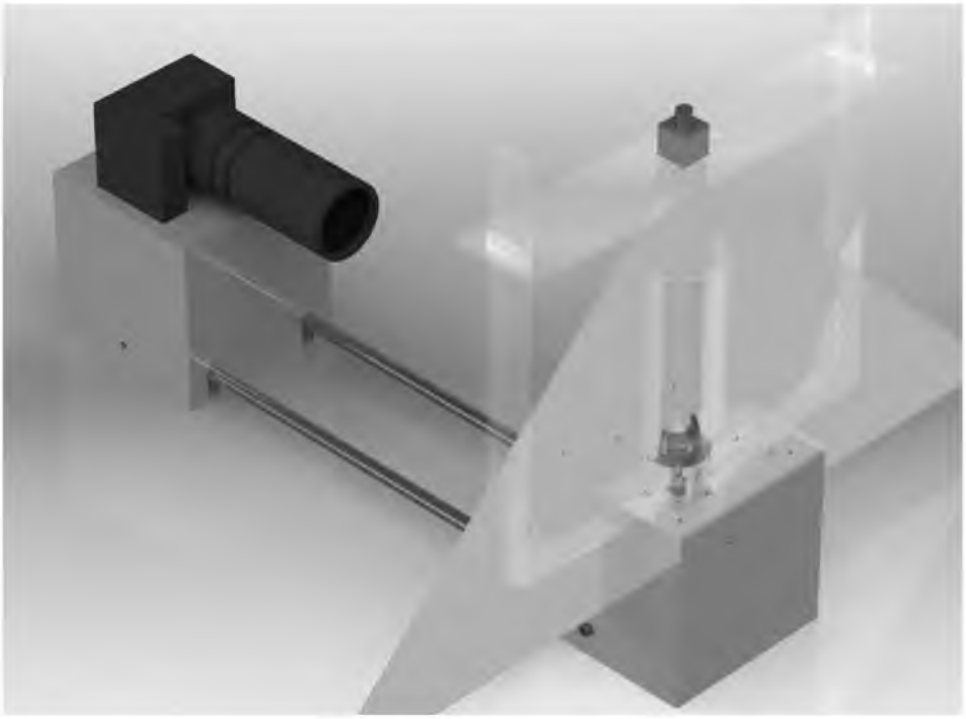

Figure 2.4 The custom stabilization and alignment fixture holds the high speed camera (upper left corner) directly in line with the center of the prototype bioreactor (lower right corner). An acrylic framework ensures that the planar laser (upper right corner) is aligned with the center plane of the reactor vessel.

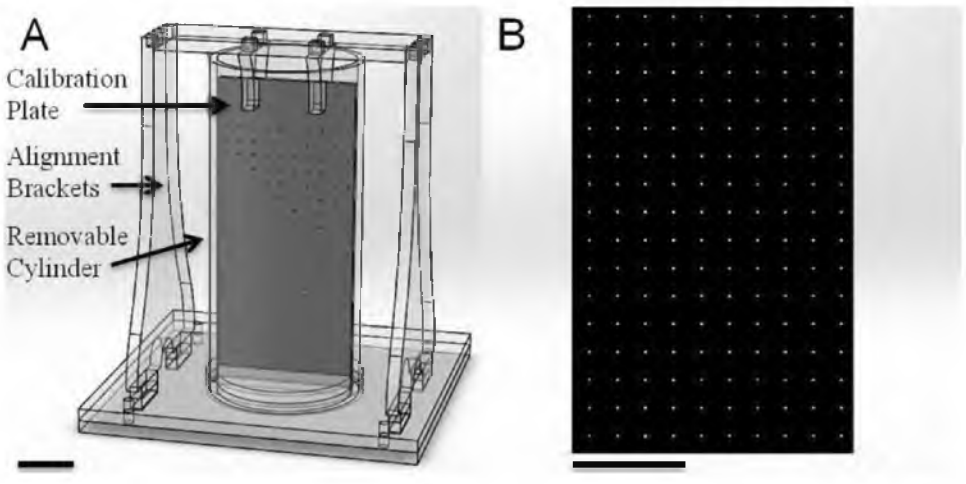

Figure 2.5 Schematic of the particle image velocimetry (PIV) calibration system comprising (A) an acrylic base and framework with a removable cylinder, and (B) an opaque calibration plate with backlit 0.3 mm holes spaced 3.175 mm in the horizontal and vertical directions. Scale bar = 50 mm.

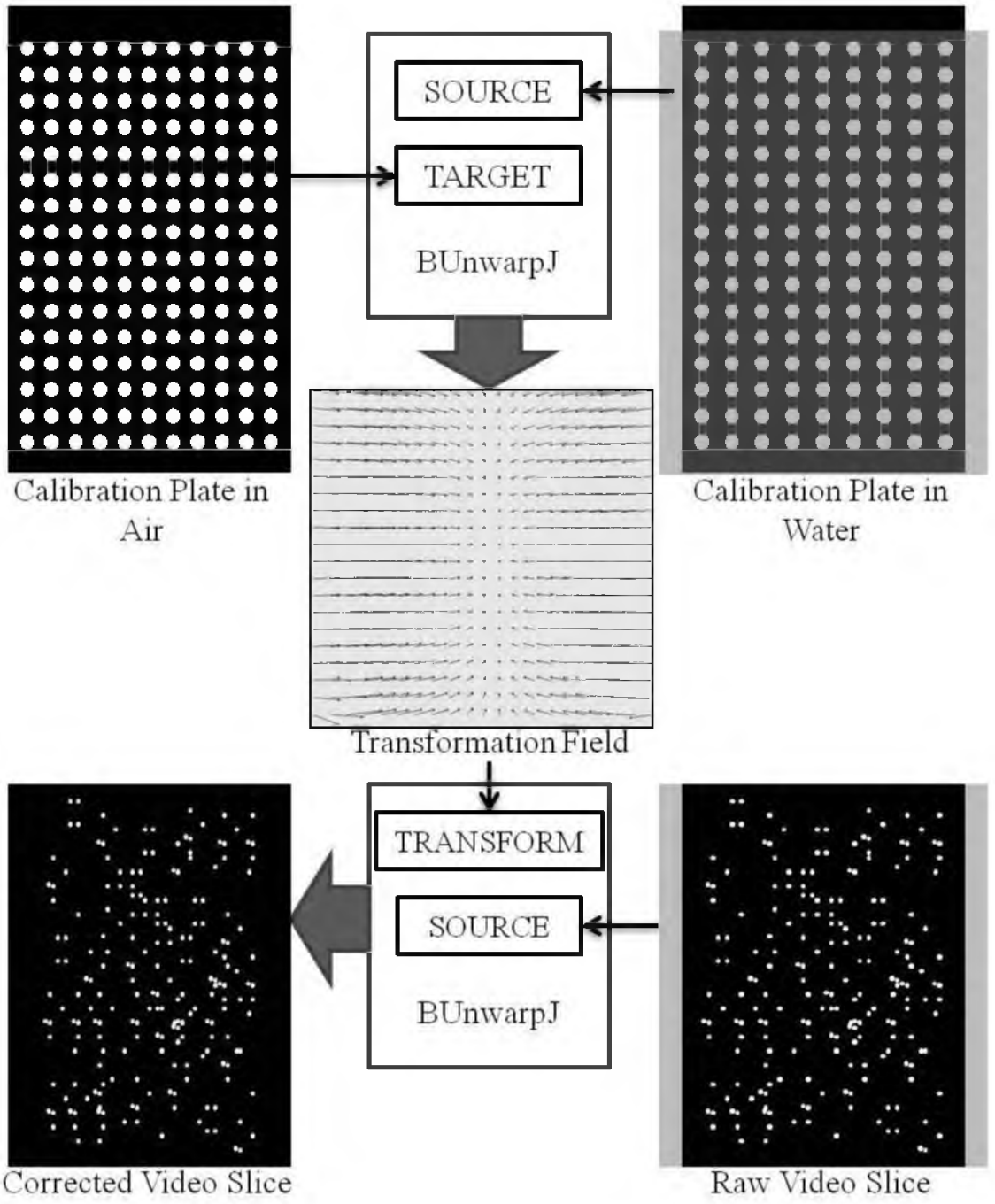

Figure 2.6 The refraction correction process uses BUnwarpJ to create and elastic transformation field from 'source' and 'target' images. This transform is then applied to the raw video slices to relocate the fluoresced particle to their true locations.

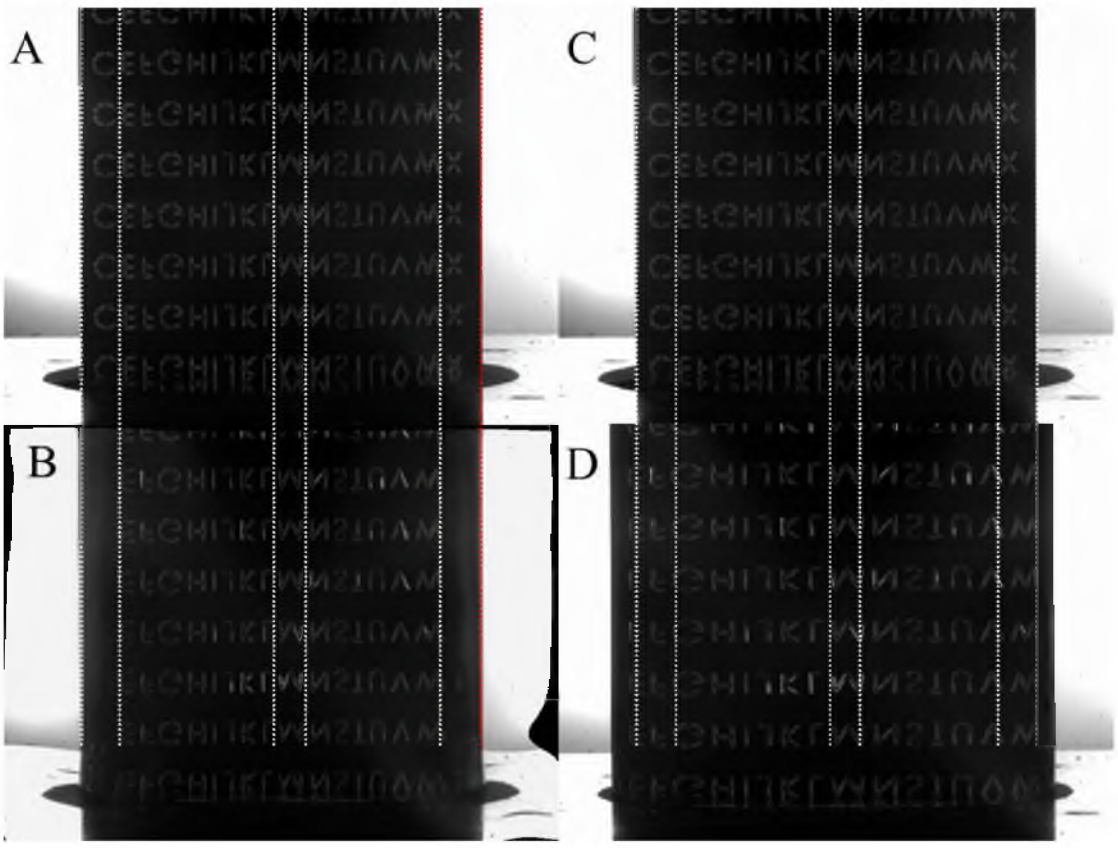

Figure 2.7 The effect of the barrel distortion is seen when the raw images are compared to the corrected images. (A) The letter sequence in air without any refraction is aligned with the corrected image (B) directly below. In contrast, the same letter sequence in air (C) cannot be aligned with (D) the letter sequence image distorted by the water and acrylic.

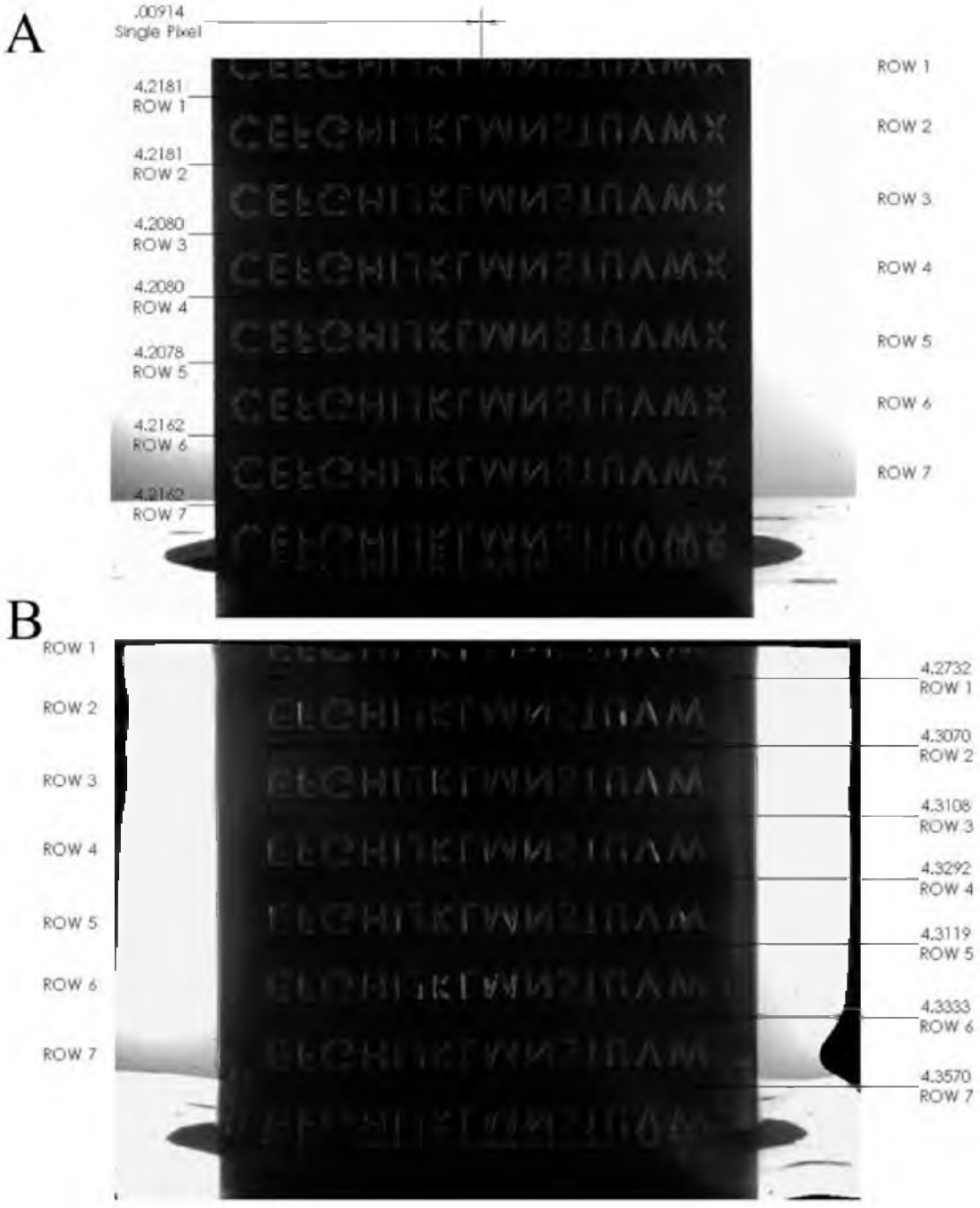

Figure 2.8 The quantitative comparison of the calibration. (A) The maximum image distance between the "E" and "W" letters is measured for all seven visible rows on the undistorted image. (B) The maximum image distance between the "E" and "W" letters is measured for all seven visible rows on the corrected image.

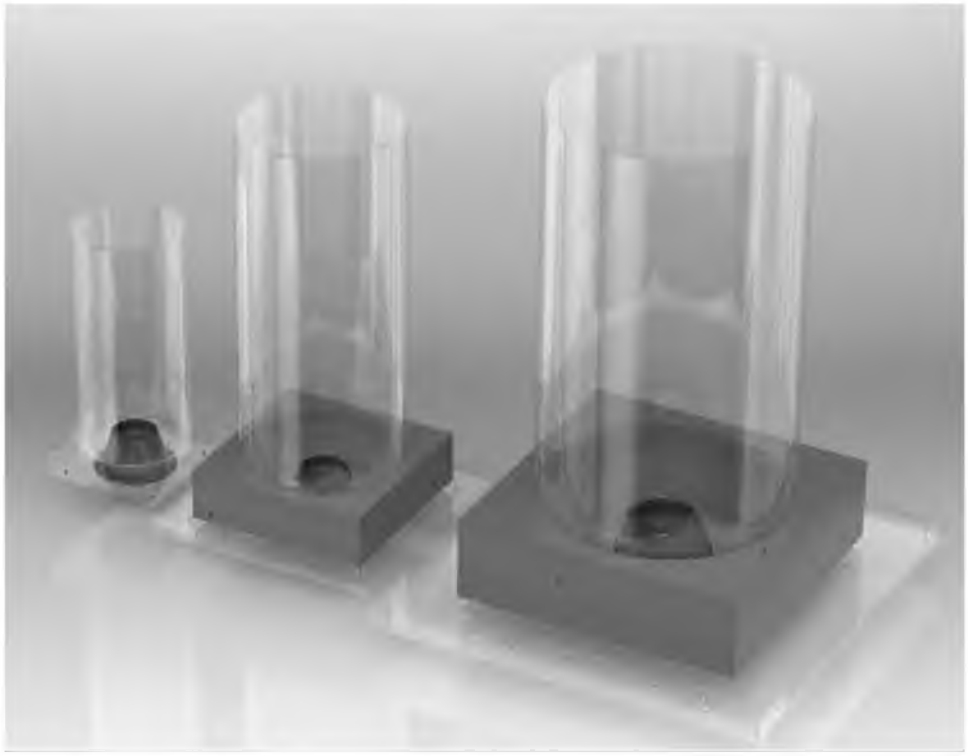

Figure 2.9 Three reactor sizes were fabricated to examine the scalability of the novel mixing design. From left to right, the sizes were 125V, 500V, and 1000V with dimension as seen in Table 2.3

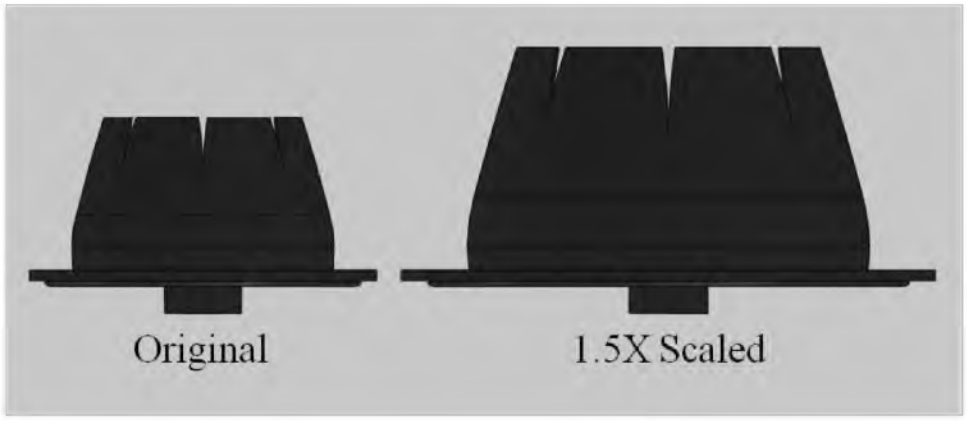

Figure 2.10 Relative size of the 1.5 times scaled silicone diaphragm (right) as compared to the original size (left). The original diaphragm was used to actuate the 125V and 500V reactor sizes. The scaled diaphragm was used to actuate the 1000V reactor.

CHAPTER 3

RESULTS

Novel Biomimetic Mechanism Flow Characteristics Quantified Using PIV

A novel silicone diaphragm incorporating biomimetic elements was successfully designed and fabricated. This diaphragm was attached to a custom bioreactor with a linear actuator and was verified to withstand the specified deformation from the upstroke and downstroke. The reactor was filled with water and achieved continuous actuation without noticeable leaks. The leak test fluid was replaced with 150 ml of distilled water with suspended fluorescent beads for flow visualization. The system was initiated and allowed to run for 10-15 minutes to ensure that fluid movement within the vessel was solely caused by the action of the novel mixing mechanism design. A global steady state was visually confirmed before recording the high speed video.

The image transformation process was successfully applied to the prepared image stack and was then input into PIVlab. The PIV algorithm was successfully completed and the mean flow of each actuation cycle was computed. The mean velocity magnitude, Figure 3.1, reveals a centralized column of upward flow through the vessel.

The flow reaches the upper boundary layer of the fluid volume and diverges radially toward the edges where momentum and gravity combine to slowly recycle the fluid mass down to the vessel bottom to supply the upward column. The mean horizontal component of the velocity was 0.08 mm/s ± 0.44 mm/s, suggesting that the horizontal flow occurring at the top and bottom of the vessel are balanced radially and produce a consistent, uniform centralized flow. The mean vertical component of the velocity, Figure 3.2, was 0.37 mm/s ± 1 mm/s with a maximum upward speed of 2.06 mm/s localized in the central flow column and the maximum downward speed of -0.93 mm/s found near the radial edge.

This flow pattern of a rising central flow which diverges and returns radially down the vessel edges is further exhibited in the streamlines of the mean flow, which show the direction any giving fluid element will travel at any point throughout the vessel space, Figure 3.3. The visualized cross section is located on the central plane of the cylindrical vessel; therefore a 360° rotation of the cross section about its midline is representative of the three-dimensional flow. By looking at the vorticity (Equation 2.3) and its gradient, the locations of the general vortices in the flow are visible, as seen in Figure 3.4. Once again, we see a vortex ring which has an upward moving inner column with a radially diverging return flow.

Finally, per Equation 2.1, the mean shear stress caused by the hydrodynamic environment can be visualized throughout the flow, see Figure 3.5. The maximum shear stress seen in the mean flow was 0.00161 dynes/cm^2. The higher magnitude stresses were localized at the interface region where the central columnar flow interacts with the slower moving fluid as you move radially outward from the upward flow to the

descending flow, reference Figure 3.1. The maximum and minimum stresses are similar in magnitude, suggesting symmetrical and predictable flow.

Scaled Vessels Maintain Flow Characteristics

The same calibration, steady state achievement, and video capture were successfully completed for all volume intervals for each of the three vessels sizes (125V, 500V, 1000V). Qualitative observation of the steady state found that the flow profile remained constant at all volumes and scales such that a centralized columnar upward flow was seen from the actuating diaphragm to the upper boundary layer of the fluid/air interface. Once the upward flow reached the top of the fluid it diverged radially and recirculated to the bottom along the radial edge of the vessel.

The mean velocity magnitudes and maximums are displayed in Table 3.1 and are graphically compared to the values seen in the 150 ml vessel in Figure 3.6. The mean and maximum velocity values for each steady state volume mean are plotted in Figure 3.7 as a function of volume and vessel size. All the mean velocity magnitude profiles are seen for the 125V, 500V, and 1000V in Figures 3.8-3.11.

The similarity of flow across all volumes and sizes is evident through qualitative comparison of the streamlines, Figures 3.12-3.14. Furthermore, the streamlines show that all regions within the vessel are included in the flow profile and experience mixing motions.

A look at the instantaneous streamline profile of the flow for any given volume or size reveals a unique element of multiple counter-rotational vortices. This phenomenon is evident in a sample frame from the 900 ml volume in the 500V vessel,

Figure 3.15. Multiple vortices are visible at various heights along both sides of the centralized columnar flow. Additionally, two of the adjacent vortices are counter-rotational which is characteristic of starting and stopping vortices. These vortices are present in the swimming wake of jellyfish and functionally aid mixing by sucking adjacent fluid into the centralized column. This increases the efficiency of each actuation stroke.

Finally, examination of the shear stress profiles for all volumes and sizes, Figures 3.16-3.18, reveals that the shear profile and magnitude match those seen in the original 150 ml size design. As the design is scaled to larger sizes, Figure 3.19 shows that the maximum mean shear stress remains relatively unchanged within a 0.002 $\frac{dynes}{cm^2}$ range.

Table 3.1 Scale-Up Velocity Magnitudes

Size	Mean (m/s)	Max (m/s)
125V	0.00051 ± 0.00023	0.00283
500V	0.00065 ± 0.00021	0.00343
1000V	0.00069 ± 0.00021	0.00343
All Scales	0.00063 ± 0.00021	0.00343

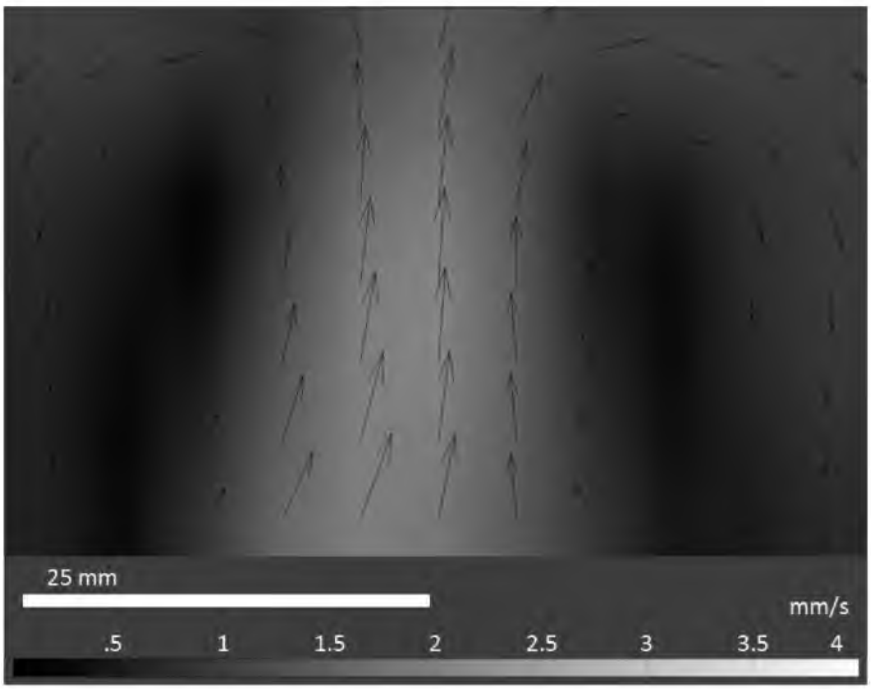

Figure 3.1 The steady state mean velocity field within the 150 ml reactor. A centralized upward flow is visible with a descending return flow located at the edges of the vessel.

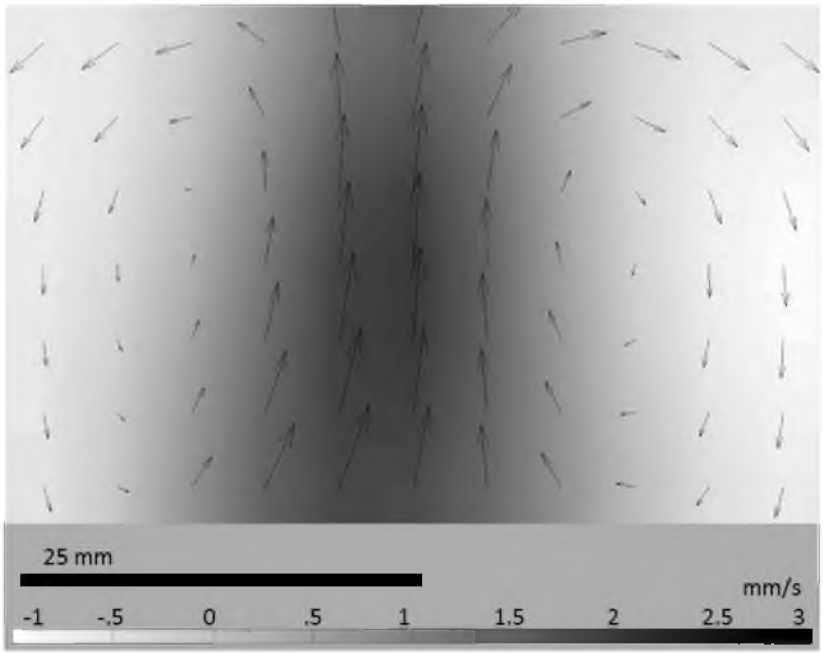

Figure 3.2 The steady state mean vertical velocity field of the 150 ml reactor. A centralized upward flow is visible with a descending return at the edges of the vessel.

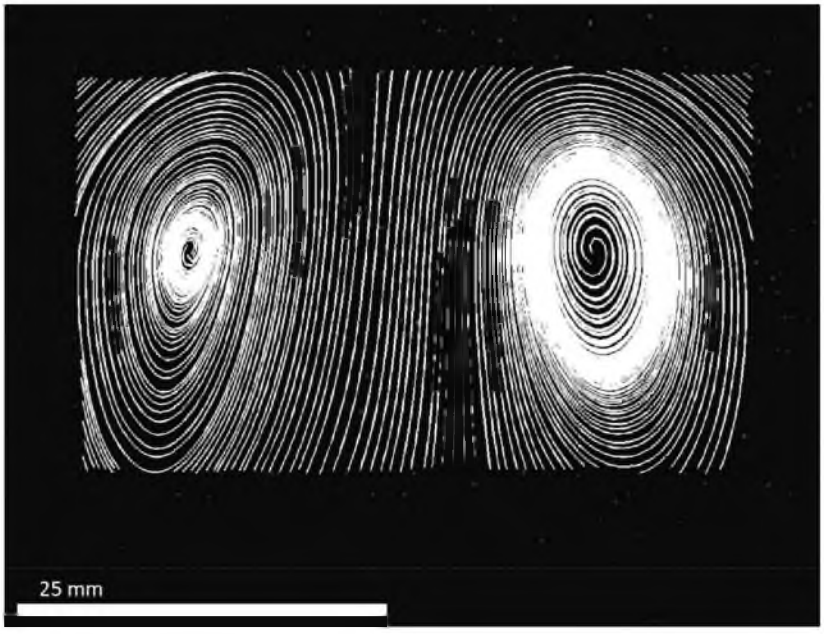

Figure 3.3 Streamlines in the 150 ml steady state flow show the cross section of a vortex ring.

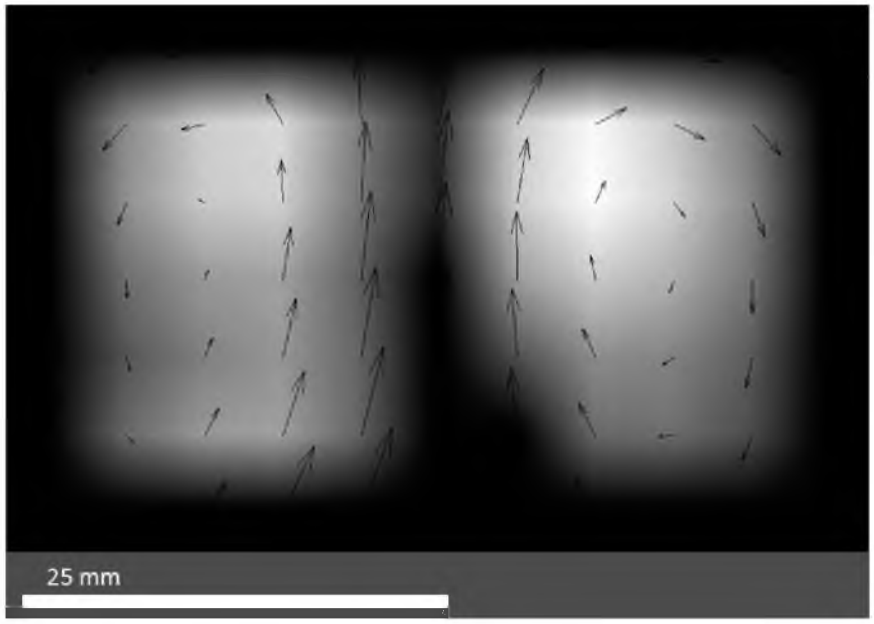

Figure 3.4 Vortex location is highlighted to show areas included in vortex circulation within the 150 ml reactor at steady state.

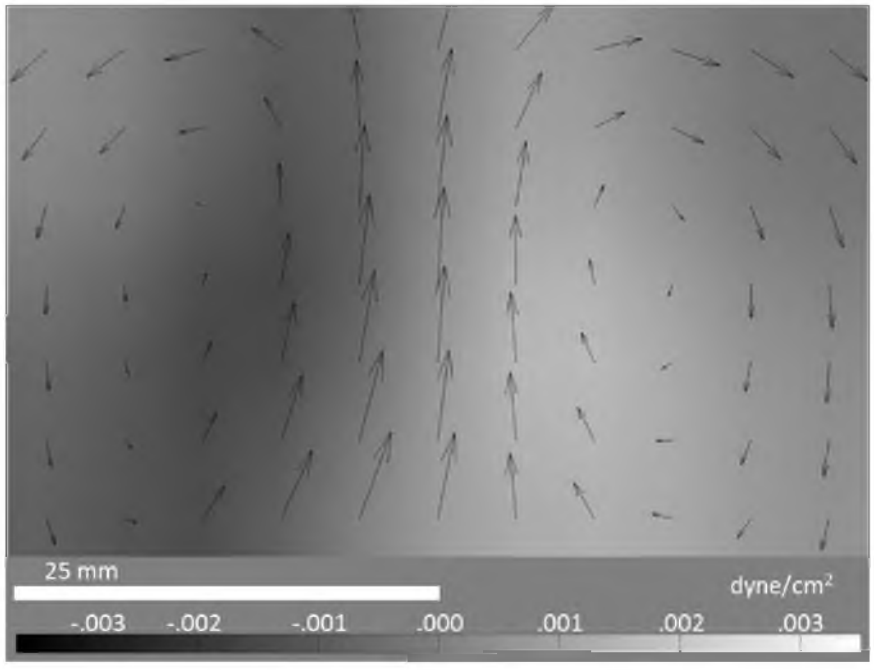

Figure 3.5 **The mean shear stress within the 150 ml reactor shows low shear homogeneity throughout the vessel.**

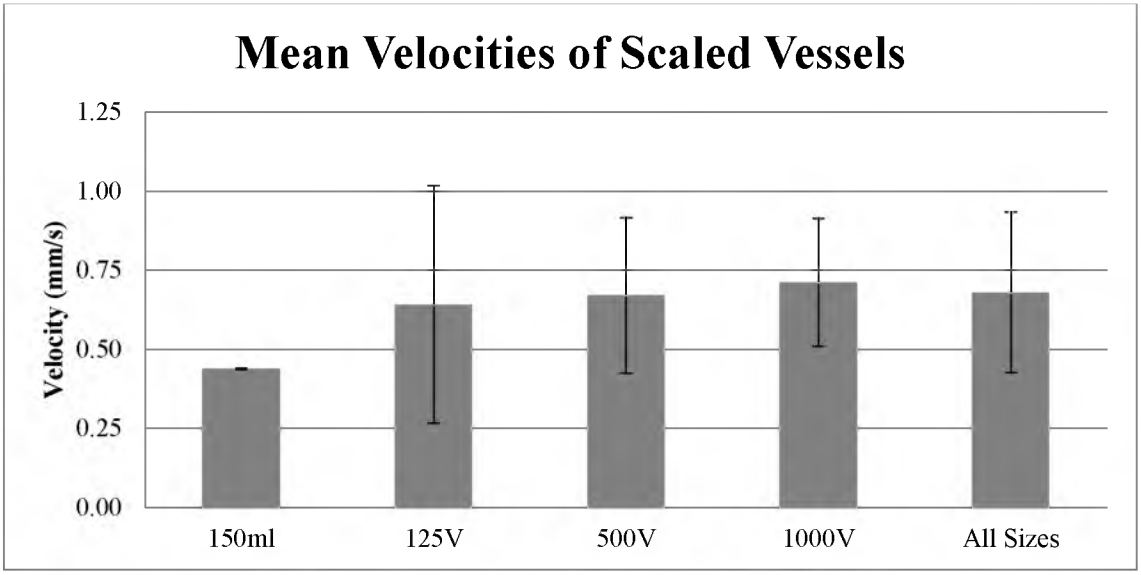

Figure 3.6 The mean velocity magnitude within the increasing sizes shows the mean to remain 0.5 mm/s ± 0.25 mm/s.

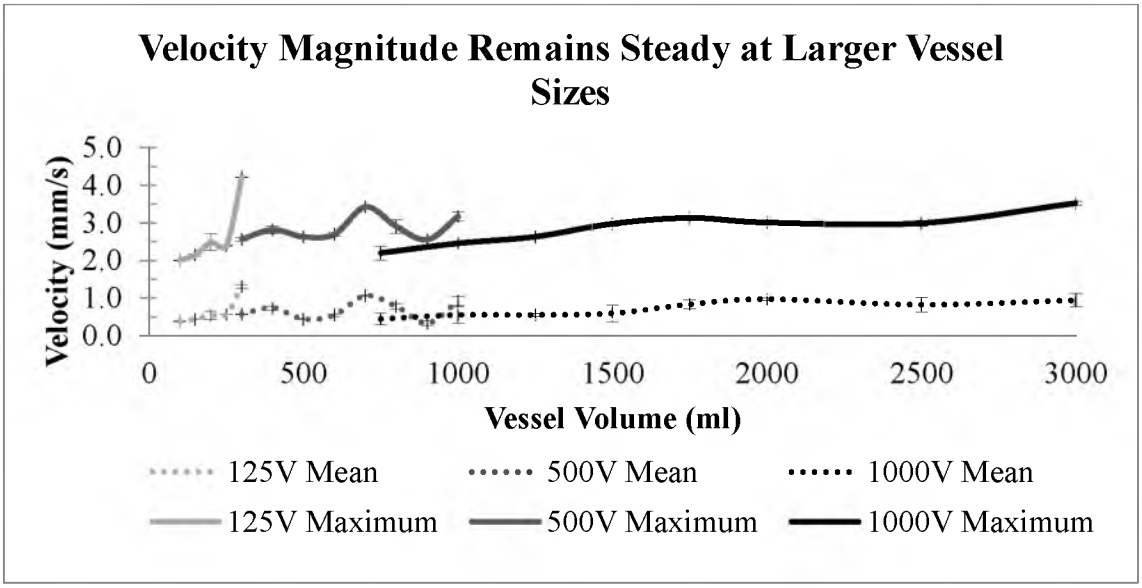

Figure 3.7 The 125V, 500V, and 1000V vessel sizes remain comparatively the same as the reactor is scaled up.

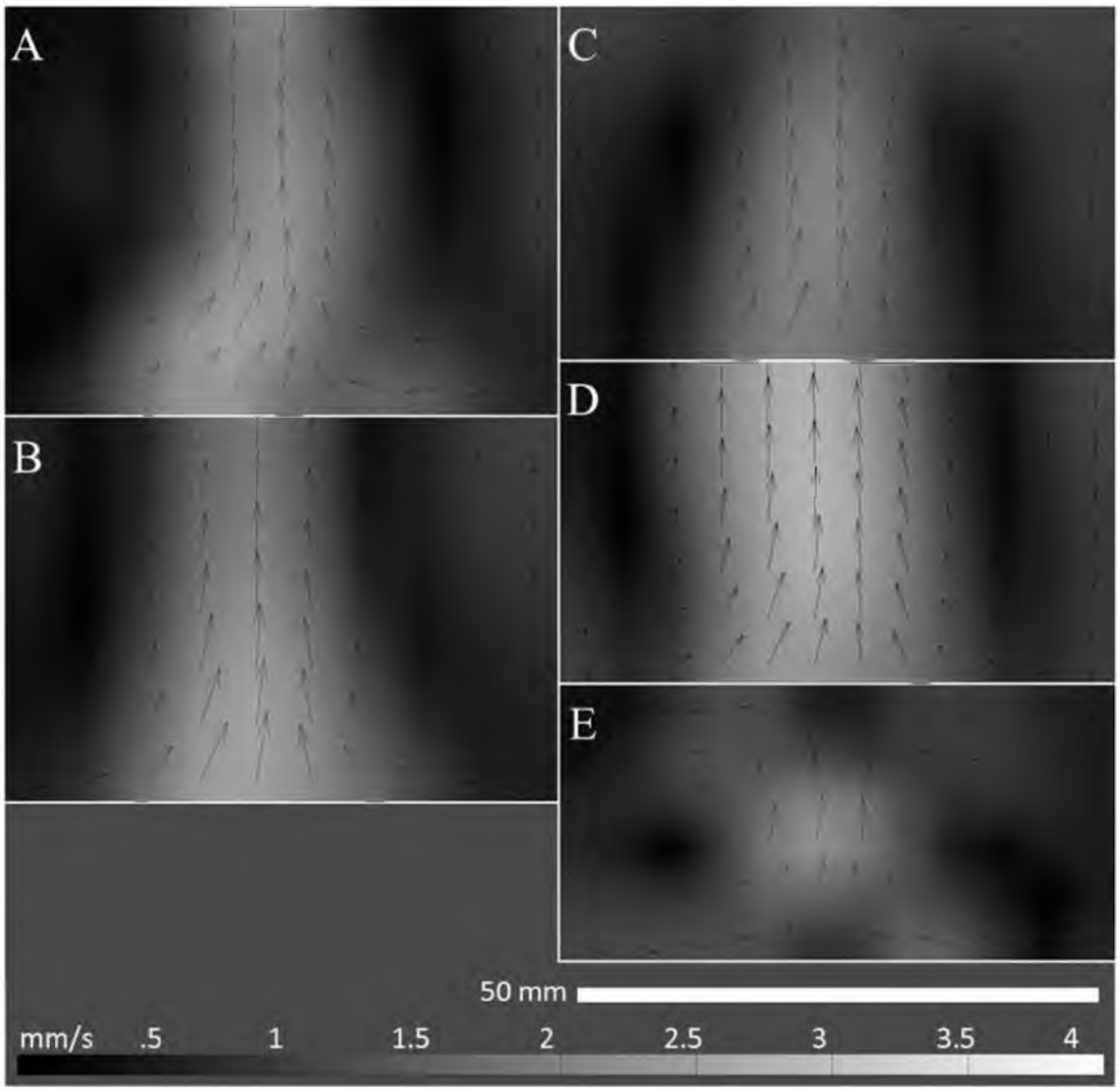

Figure 3.8 The steady state mean velocity fields within the 125V reactor for all tested volumes. A centralized upward flow is visible with a descending return flow located at the edges of the vessel. When the upper fluid boundary is higher at increased volumes, (A) 300 ml and (B) 250 ml, a centralized columnar flow is evident. At lower volumes, (C) 200 ml, (D) 150 ml, (E) 100 ml, the fluid boundaries near the core circulation of the vortex ring.

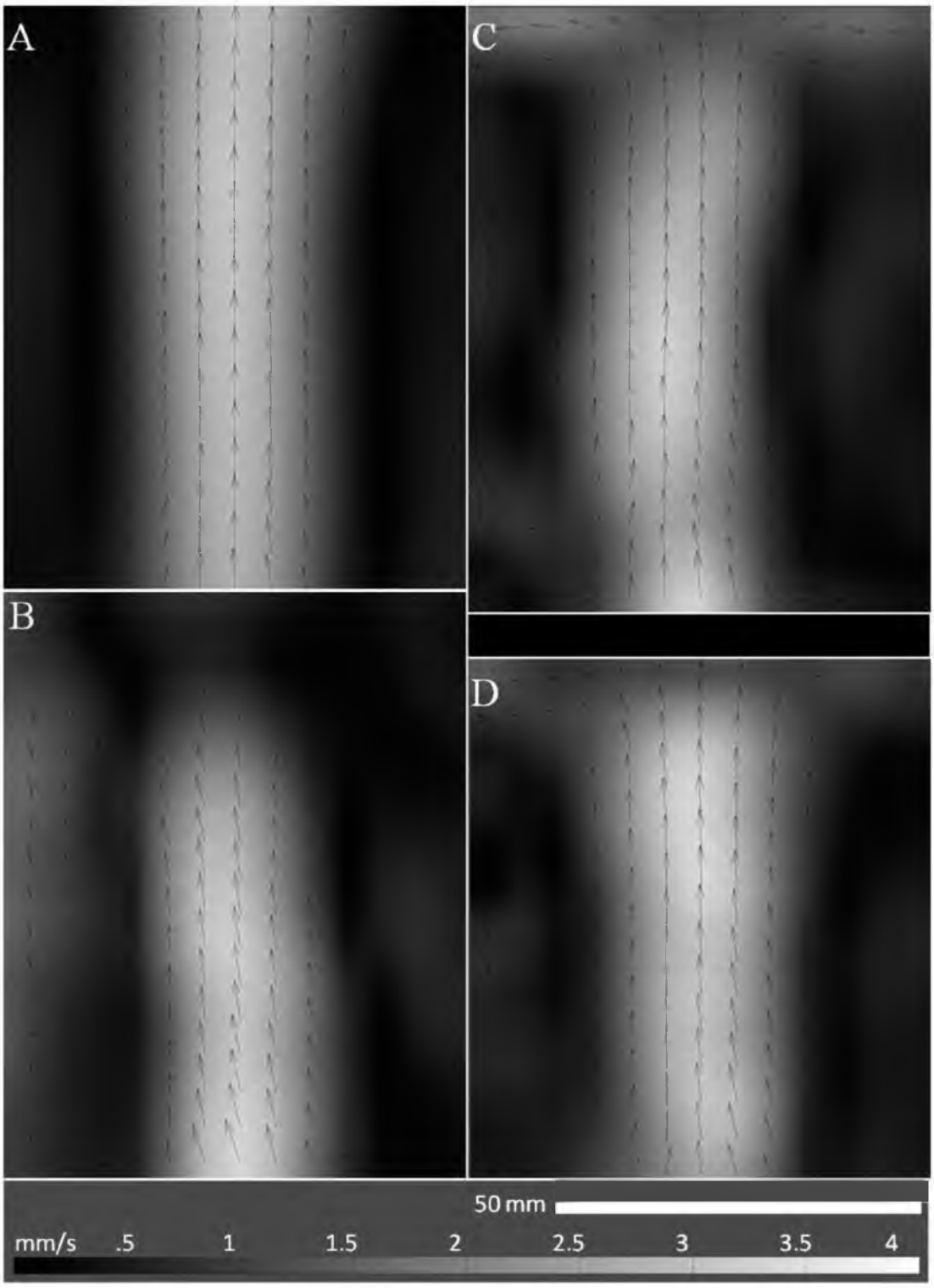

Figure 3.9 The steady state mean velocity fields within the 500V reactor show a centralized upward flow with a descending return flow located at the edges of the vessel. (A) 1000 ml, (B) 900 ml, (C) 800 ml, (D) 700 ml.

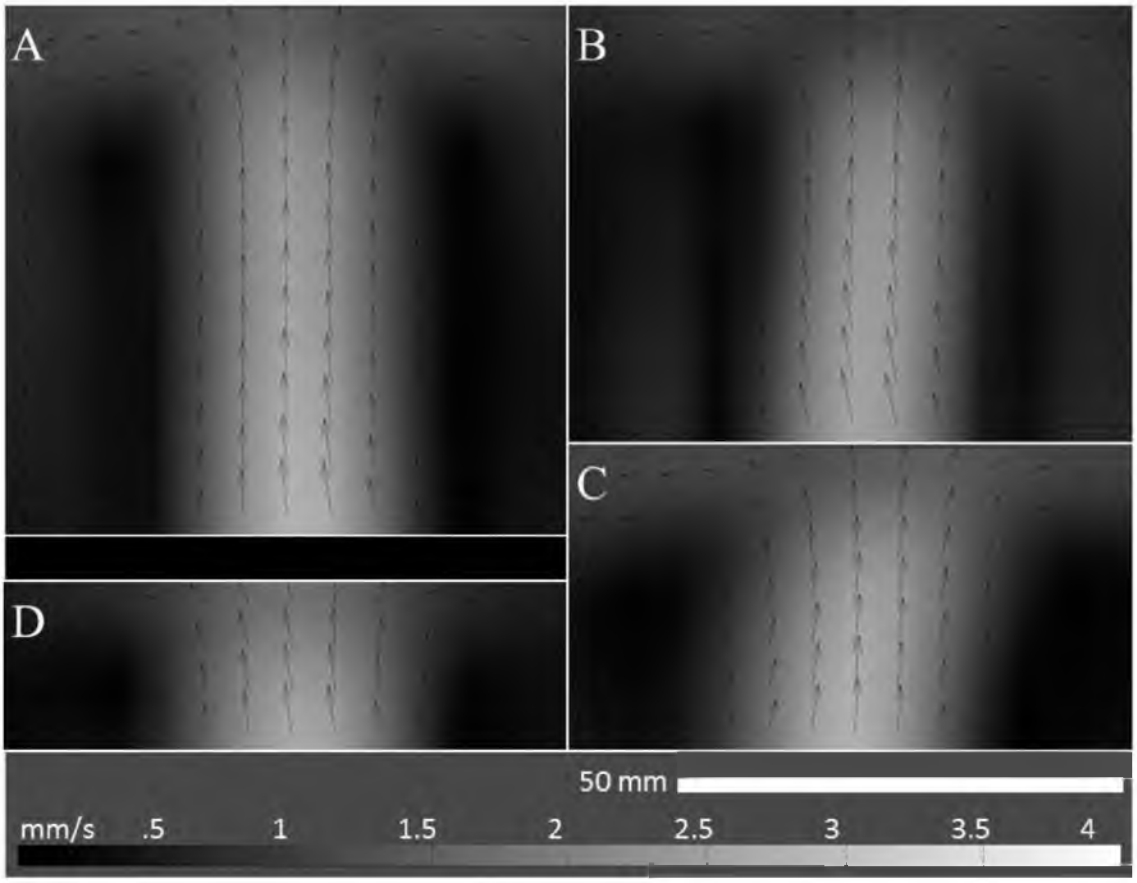

Figure 3.10 The steady state mean velocity fields within the smaller volumes of the 500V reactor also show a centralized upward flow with a descending return flow located at the edges of the vessel. (A) 600 ml, (B) 500 ml, (C) 400 ml, (D) 300 ml.

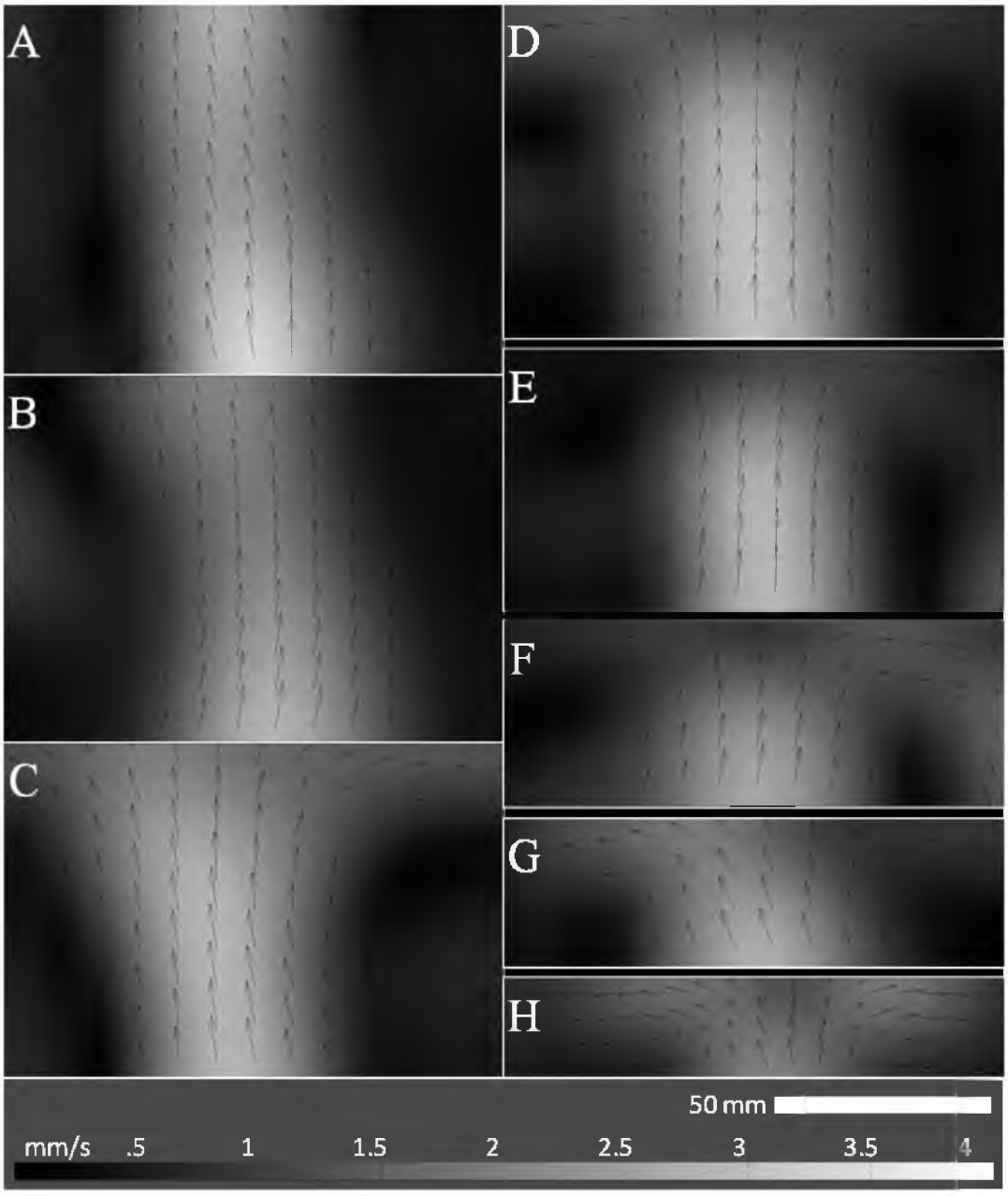

Figure 3.11 The steady state mean velocity fields within the 1000V reactor for all tested volumes. A centralized upward flow is visible with a descending return flow located at the edges of the vessel. Volumes tested include (A) 3000 ml, (B) 2500 ml, (C) 2000 ml, (D) 1750 ml, (E) 1500 ml, (F) 1250 ml, (G) 1000 ml, and (H) 750 ml.

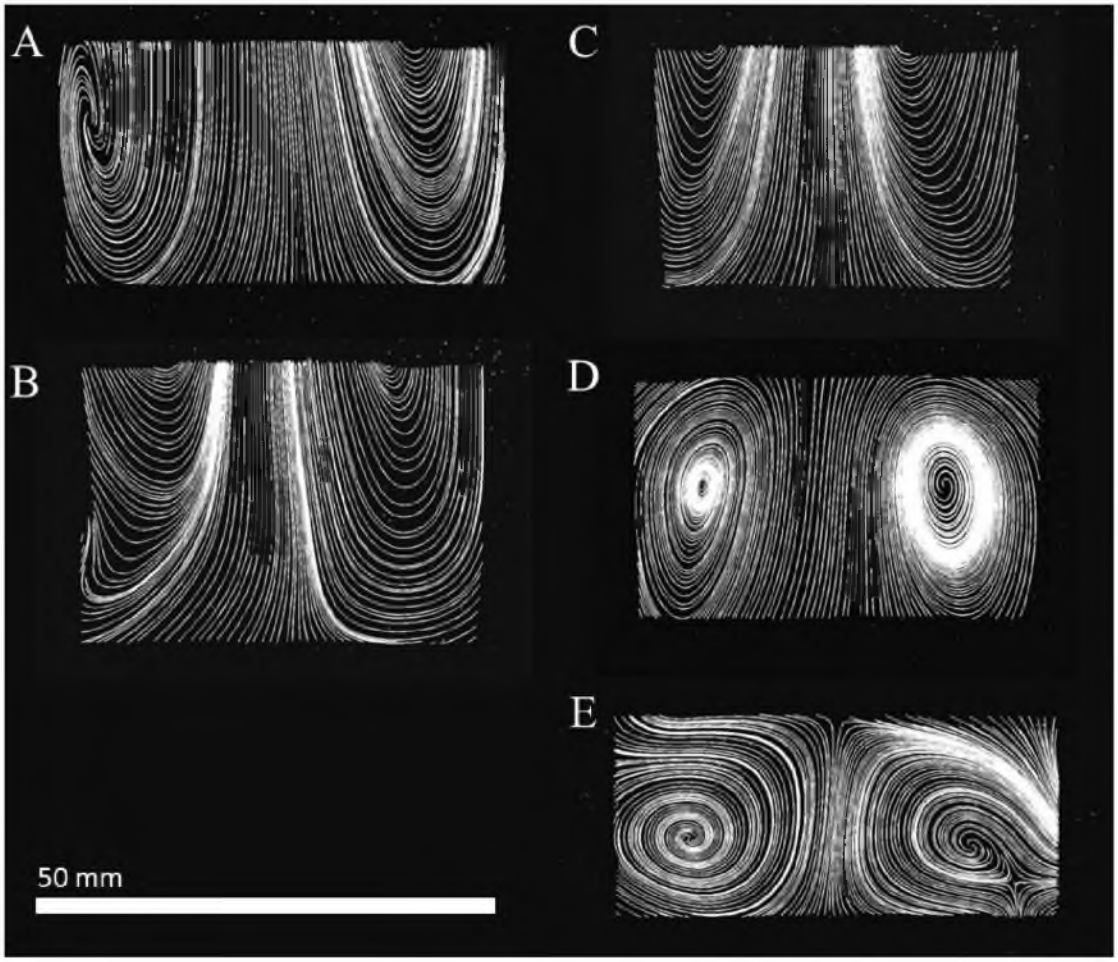

Figure 3.12 The steady state streamlines within the 125V reactor for all tested volumes. Large rotations are seen with a centralized upward flow at all sizes. (A) 300 ml, (B) 250 ml, (C) 200 ml, (D) 150 ml, (E) 100 ml.

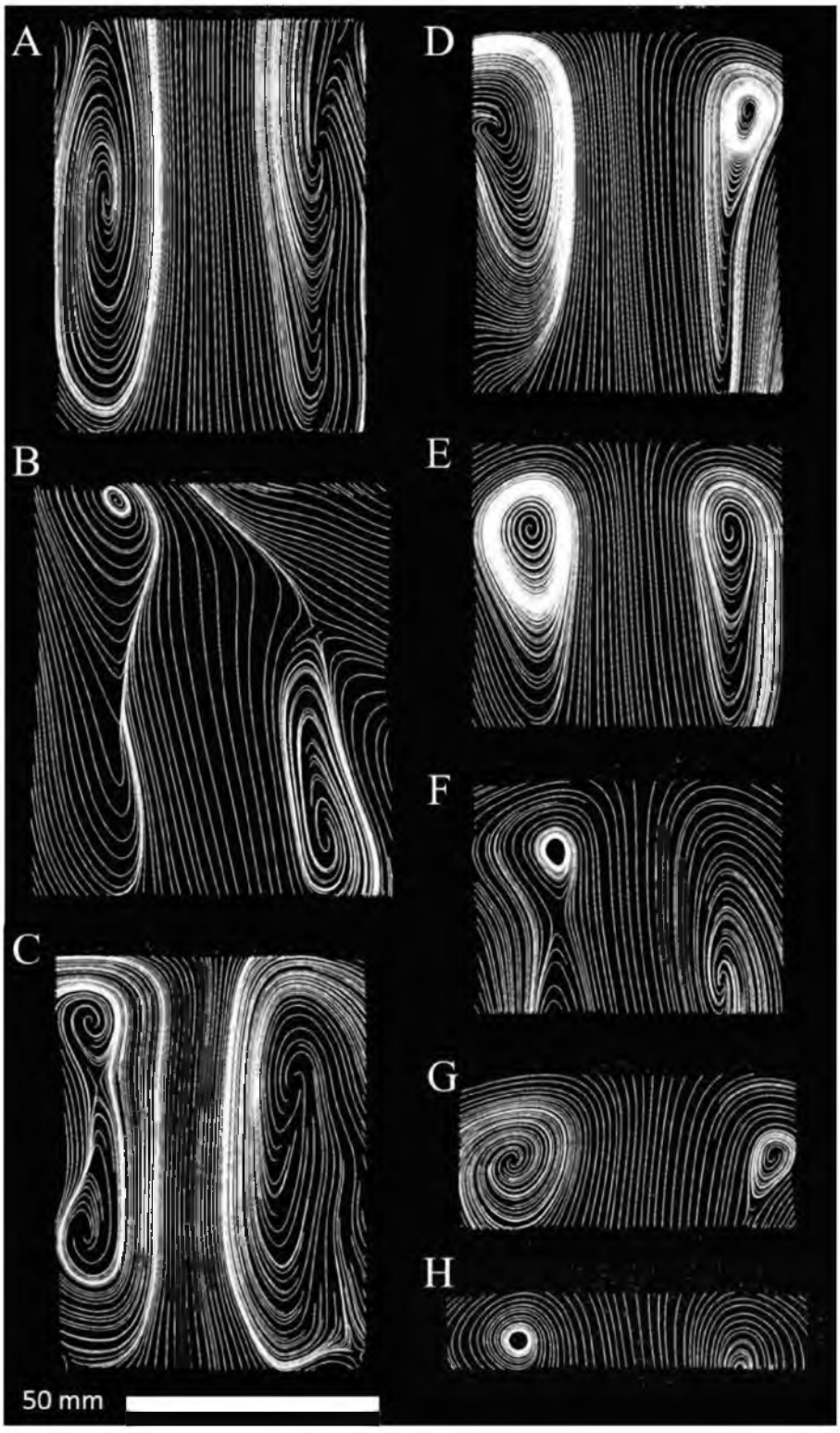

Figure 3.13 500V steady state streamlines. (A) 1000 ml, (B) 900 ml, (C) 800 ml, (D) 700 ml, (E) 600 ml, (F) 500 ml, (G) 400 ml, (H) 300 ml.

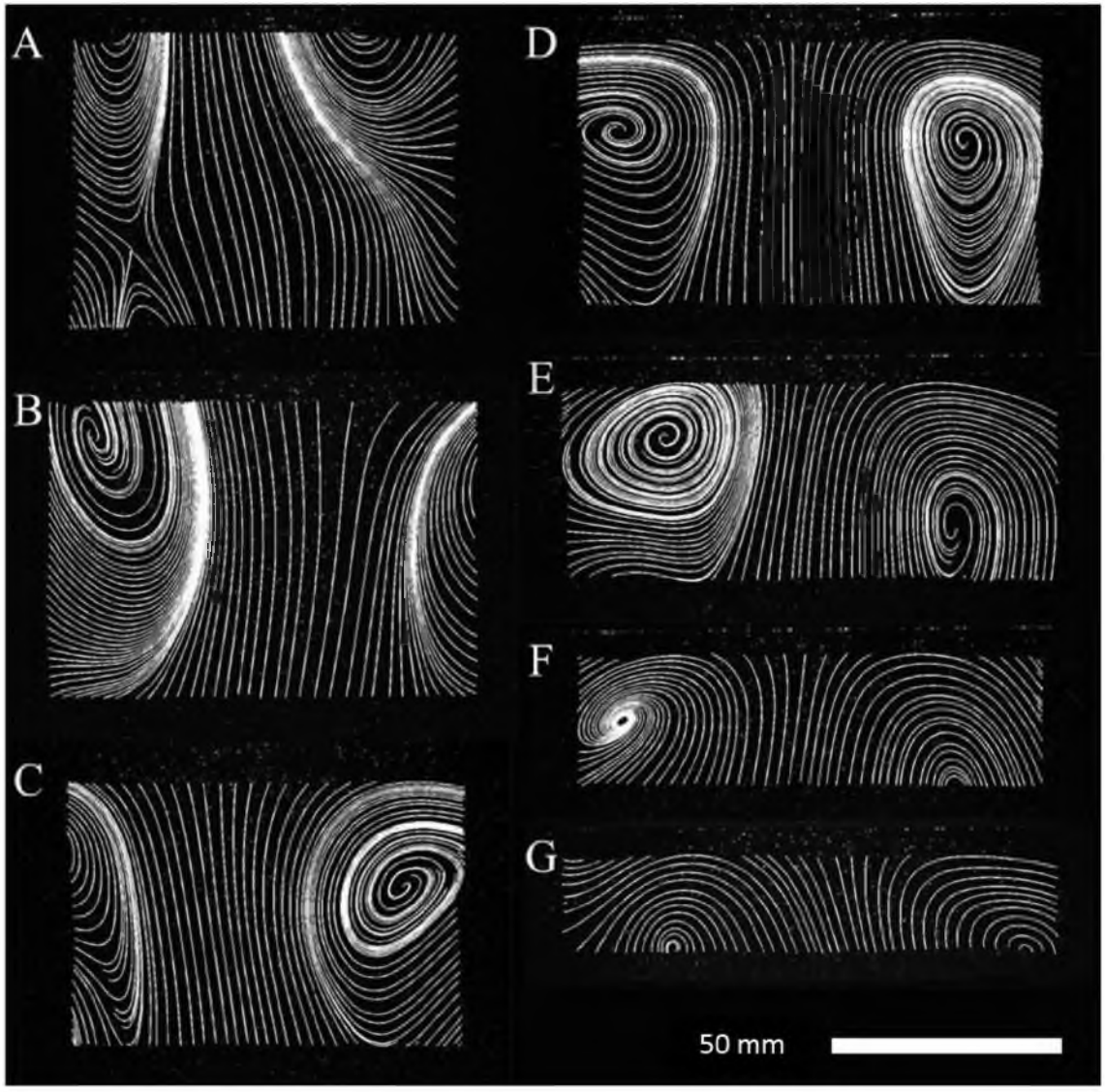

Figure 3.14 The steady state streamlines within the 1000V reactor for all tested volumes. Large rotations are seen with a centralized upward flow at all sizes. Volumes include: (A) 3000 ml, (B) 2500 ml, (C) 2000 ml, (D) 1750 ml, (E) 1500 ml, (F) 1250 ml, and (G) 1000 .

Figure 3.15 Instantaneous streamlines of the 900 ml volume in the 500V vessel sizes show rising vortex rings. Counter-rotational starting and stopping vortices are seen.

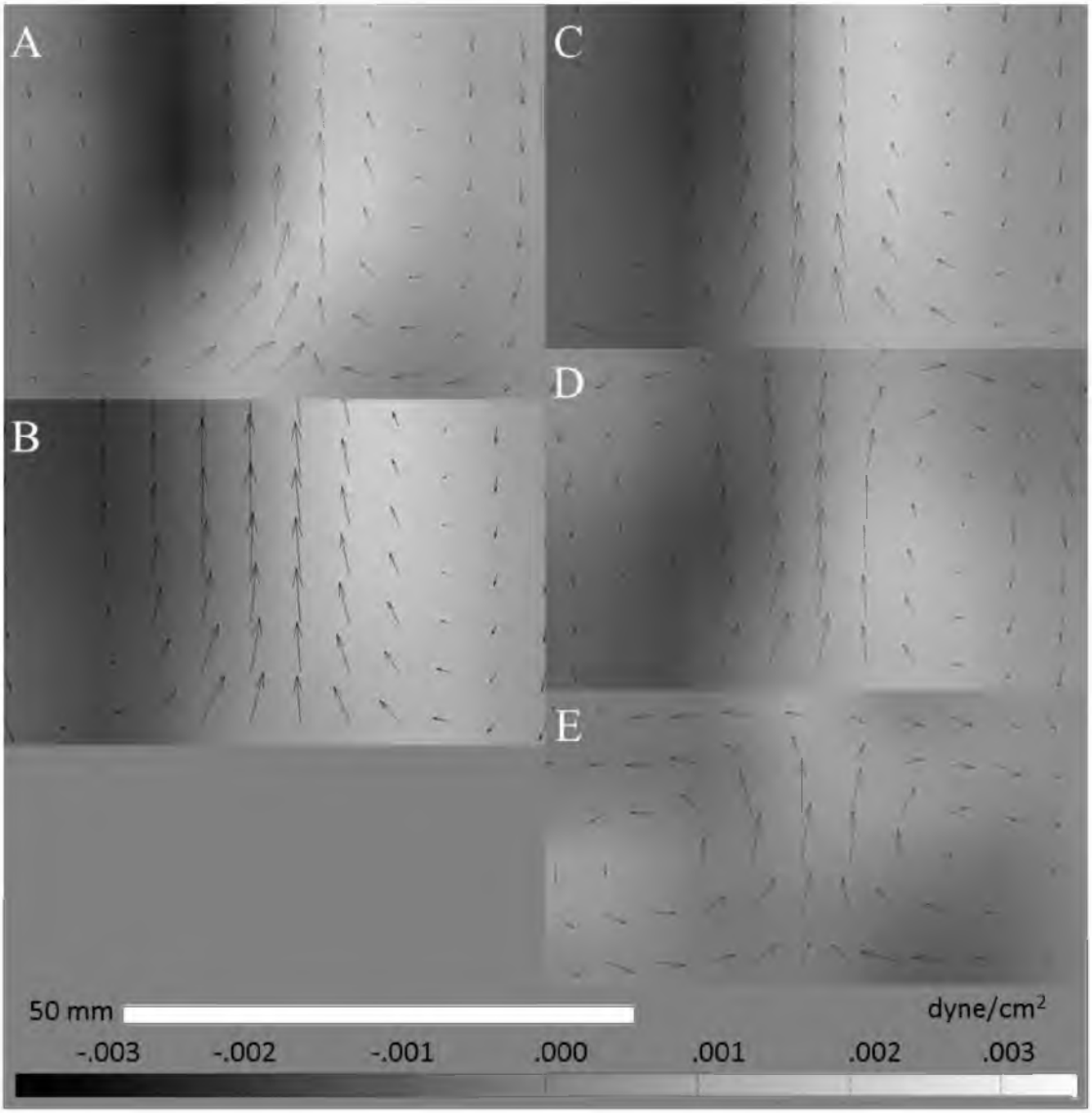

Figure 3.16 The mean shear stress within the 125V reactor shows low shear homogeneity throughout the vessel. (A) 300 ml, (B) 250 ml, (C) 200 ml, (D) 150 ml, (E) 100 ml.

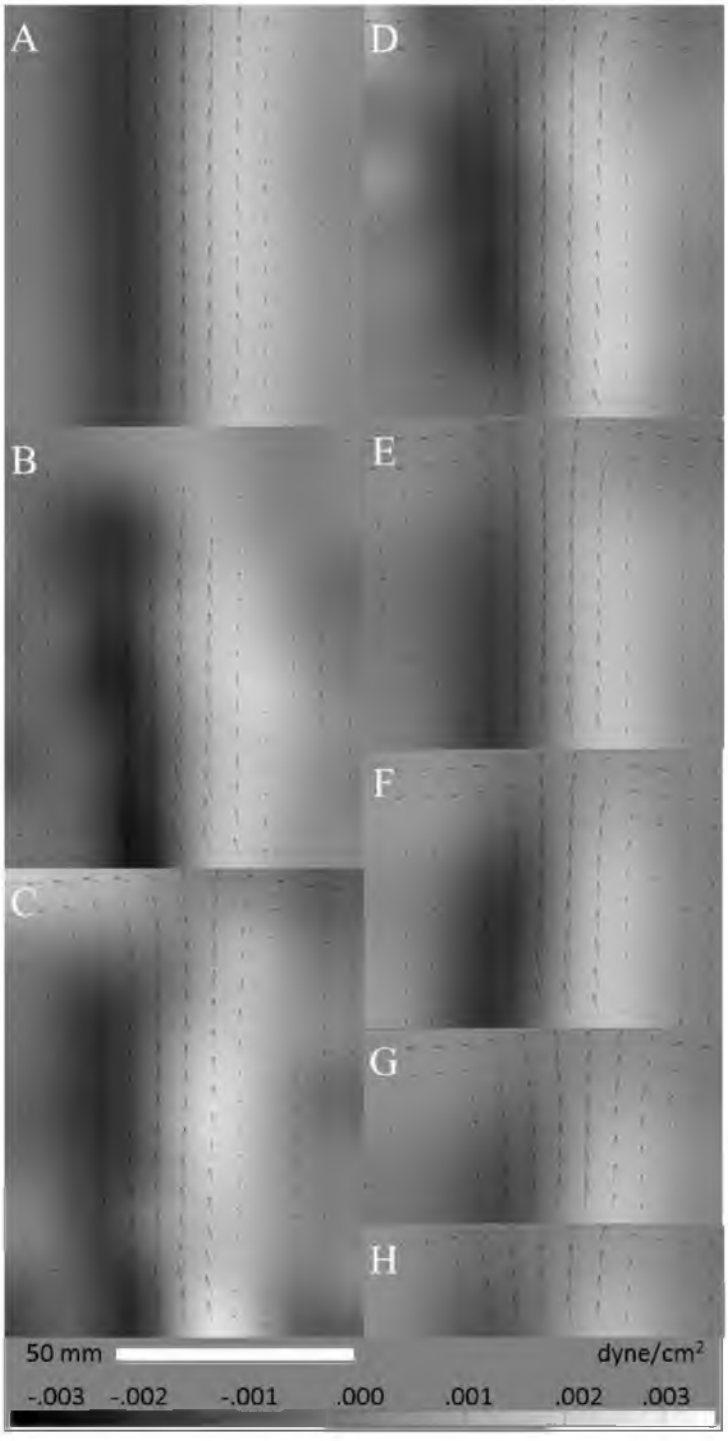

Figure 3.17 Low shear stress homogeneity in the 500V vessel. (A) 1000 ml, (B) 900 ml, (C) 800 ml, (D) 700 ml, (E) 600 ml, (F) 500 ml, (G) 400 ml, (H) 300 ml.

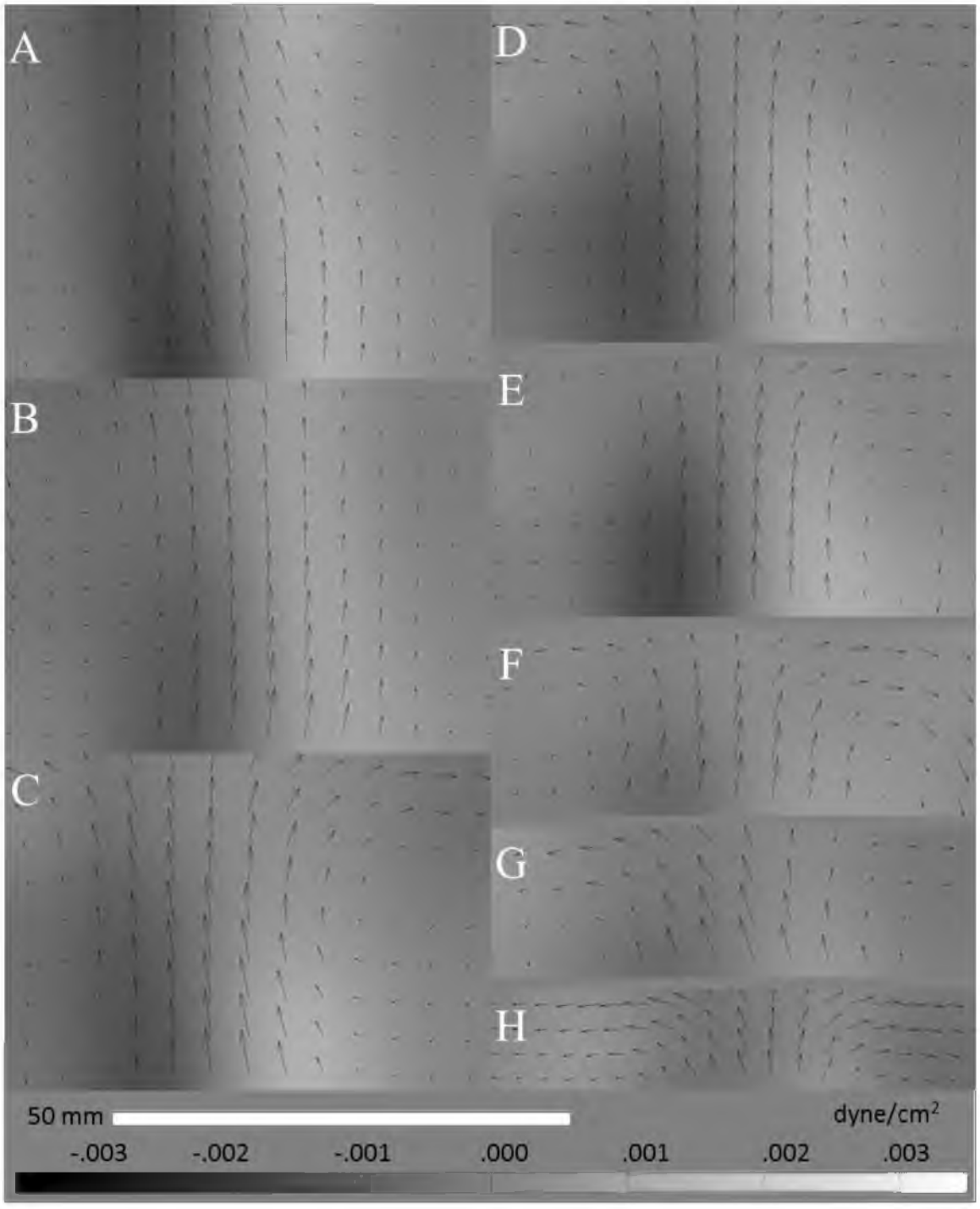

Figure 3.18 Low shear homogeneity seen throughout the 1000V vessel size. Volumes tested include (A) 3000 ml, (B) 2500 ml, (C) 2000 ml, (D) 1750 ml, (E) 1500 ml, (F) 1250 ml, (G) 1000 ml, and (H) 750 ml.

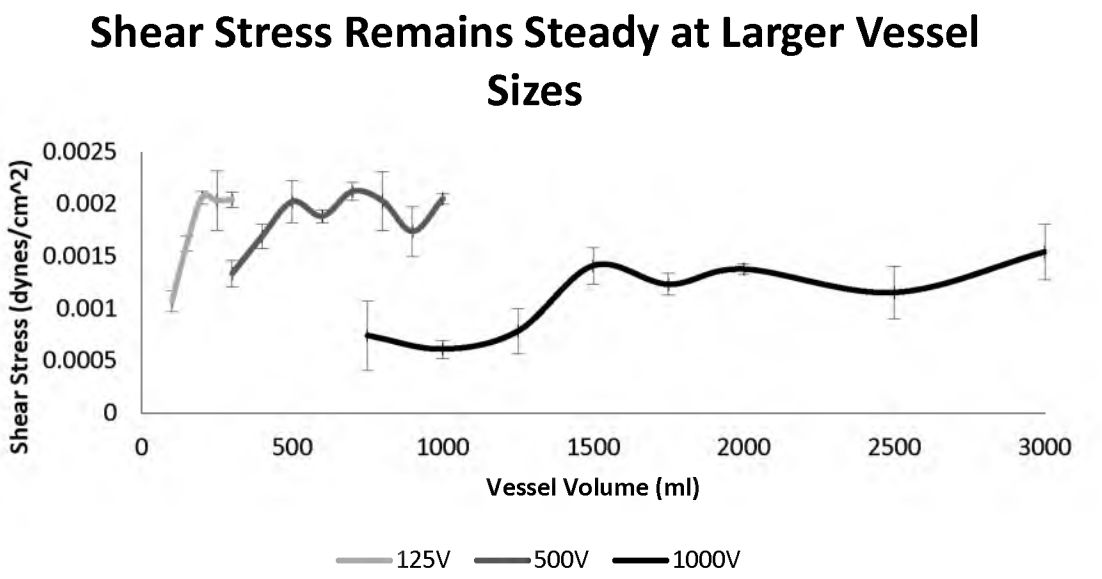

Figure 3.19 The shear stress within the vessel remains within a 0.002 $\frac{dynes}{cm^2}$ range as the design is scaled to larger sizes. Slight increases are observed in each vessel at their respective higher volumes.

CHAPTER 4

DISCUSSION

The medical industry routinely experiences paradigm shifts as break-through technologies and innovation allow for new perspectives and revolutionize treatments. In recent decades, a major treatment paradigm has been the utilization of protein based therapeutics produced through large scale cell bioprocessing [1], [2]. Regenerative medicine and tissue engineering are poised to yet again shift the paradigm of medical treatment through the application of stem cell based therapeutics. For this to occur on a clinically relevant scale, the quantity and quality of stem cell production must match that presently seen in the protein bioprocessing industry. Current bioprocess mixing technologies were not designed to meet the delicate requirements of environmentally sensitive stem cells. Furthermore, recent designs which fulfill these requirements have faced significant challenges when scaled to larger sizes.

Our goal was to develop a novel mixing system that solves both conflicting suspension design challenges; namely creating a low shear homogenous mixing environment conducive to retention of an undamaged cell and unaltered phenotype, and maintaining that mixing environment as the design is scaled to larger volumes.

Novel Biomimetic Mixing Design

The developed design incorporates both a legacy bioprocess technology and a biomimetic model. The Alternating Tangential Flow (ATF™) perfusion system marketed by Refine Technology utilizes an up and down motion to induce laminar flow across a filtration module connected to a bioreactor. Similarly, the proposed design uses this fundamental motion to create a mixing flow within a closed reactor vessel as seen in Figure 2.2.

Jellyfish propulsion has been studied by Dabiri *et al.* at the California Institute of Technology. Our design features geometric elements such as aspect ratio and structural elements such as the hinged flexible fins that contribute to the jellyfish rowing swim stroke [62]. More importantly, jellyfish create starting and stopping vortex rings on each stroke leading to an effective and efficient actuation. The fundamental schematic underlying vortex ring function is shown in Figure 4.1 [57], [59]. Instantaneous streamline analysis of the novel mixing design exhibits multiple counter-rotational starting and stopping vortices rising through the central column of the reactor flow, see Figure 3.15. As seen in jellyfish propulsion, this flow mechanism lends to highly efficient mixing by sucking in fluid along the reactor edges through the counter-rotational adjacent vortex superstructures.

Low Shear Mixing Maintained Through Scale-Up

The results seen in the 150 ml vessel successfully met the design requirements of a low shear homogenous mixing environment. In line with the project goals, these flow characteristics were maintained as the design was scaled to larger sizes. Figure 4.2

shows the maximum steady state velocity magnitudes are considerably lower than seen in impeller systems as the design is scaled [71]. The constancy of scale-up is more drastically evident when compared to the lowest shear value, 0.3 $\frac{dynes}{cm^2}$, present in impeller stirred bioreactor designs as reported by Sucosky *et al.* [64], Figure 4.3.

Limitations

The method for quantification of the mechanical dynamics within the fluid flow, particle image velocimetry, is strongly dependent on the accuracy of particle placement in successive analysis frames. Due to the refraction in the curved surface of the vessel, secondary corrective image processing was required. Error inherent in this process will propagate in the quantifying computations. Additionally, the curvature of the vessel leads to areas along the vertical walls that are not visualized. Analysis of these areas is crucial as shear forces occur at the interfaces of boundaries, namely that of the fluid flow and the static wall. Finally, particle image velocimetry uses multiple interrogation windows in the cross correlation between images. In order to successfully capture displacement vectors, a larger interrogation window with an area of 80 pixels was used. Higher resolution and accuracy would be obtained with a smaller interrogation window. This may be accomplished through increased fluorescent bead density or through a higher capture frame rate. The frame rate used was limited by the low light conditions, whereas the high speed camera used was design for well-lit capture.

Scalability was limited to 3000 ml in the 1000V vessel due to fabrication cost constraints. Additionally, the curved bases of the 500V and 1000V sizes were not

fabricated using cast acrylic as was the 125V due to cost constraints. This resulted in reduced visualization in the larger vessels.

Future Direction

Further characterization and development of the novel biomimetic mixing design is needed before this design can feasibly be utilized in a commercial setting. The design geometry and performance can be further optimized for the lowest shear and most homogenous mixing possible. The linear scaling factor of 1.5 times and the volume ranges for each vessel size can be verified through repetition of the experiments conducted herein and additional experiments could be conducted on considerably larger scales (10 L → 100 L → 1000 L).

The most important future study, however, highlights the interaction of the bioreactor performance on living stem cells in prolonged culture under full production conditions. This validation will require a sterile and sealed bioreactor system. Studies should be conducted to examine cell viability and expansion. Additionally, mesenchymal stem cells will be cultured and evaluated for phenotypic maintenance. The bioreactor would also need noninvasive sensing and real time feedback/control mechanisms to monitor and regulate the culture temperature, pH, CO_2, and dissolved O_2 levels. The incorporation of perfusion, feeding, and automated harvesting has the potential to establish this system as an industrial benchmark and will have a large impact on the cell therapy industry. These elements, in combination with the optimized mixing profile have the potential to achieve high levels of cell expansion through predictable flow environments.

In conclusion, we have used a requirements based design approach to successfully design and develop a novel proof of concept prototype that integrates the needs of delicate stem cell expansion, the legacy ATF™ system technology, and innovative biomimetic elements into a novel mixing system (Figure 4.4). The system has been shown to maintain low mean velocity and consequently low shear stresses. Furthermore, the mixing system has been successfully scaled across the 100 – 3000 ml range. This study provides the foundation for further optimization and development of the complete bioreactor system for the expansion of mesenchymal stem cells for tissue engineering and regenerative medicine.

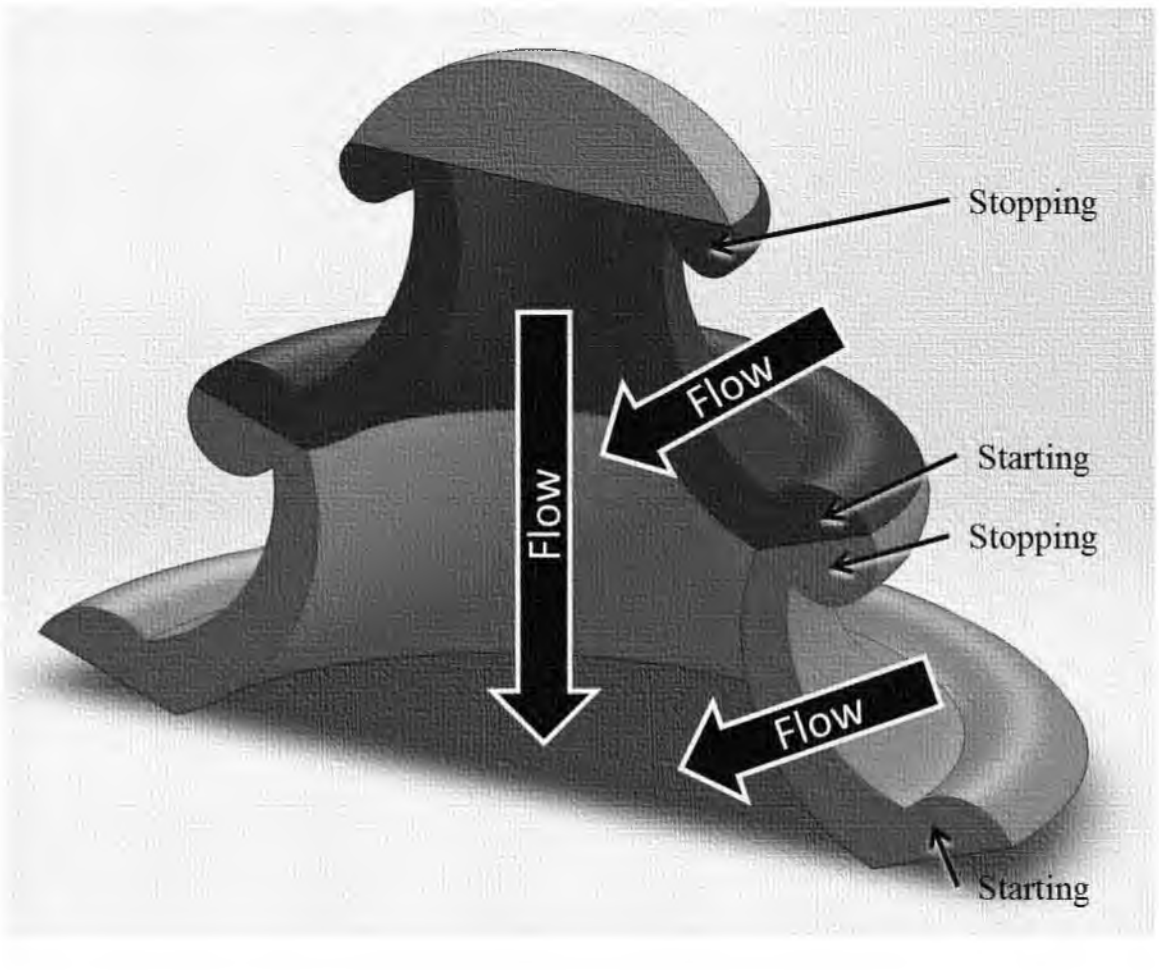

Figure 4.1 Starting and stopping vortices in the vortex wake created by the biomimetic diaphragm. Efficient mixing is facilitated by the induced flow between starting and stopping vortices. Figure adapted with permission [57].

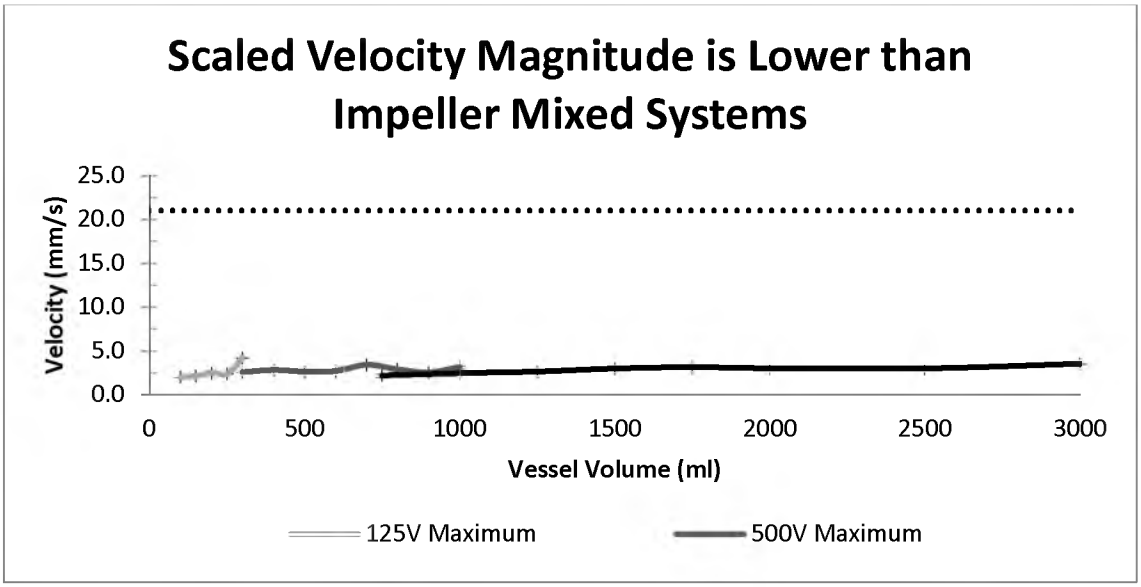

Figure 4.2 The maximum steady state velocity magnitudes remain considerably lower than seen in impeller mixed systems (Sucosky) while scaled.

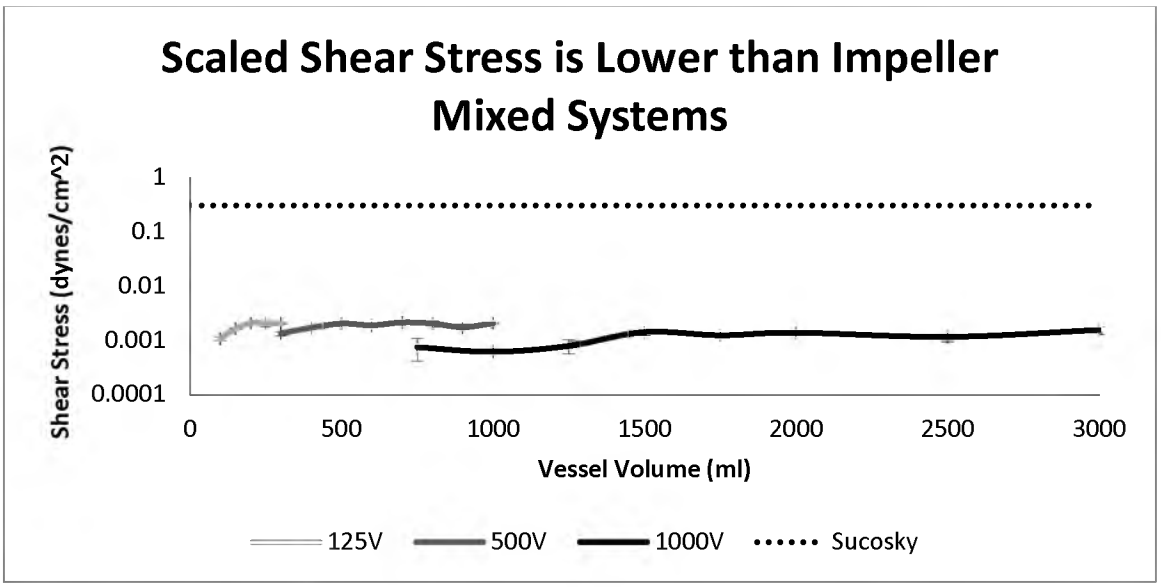

Figure 4.3 The steady state shear stress remains orders of magnitude lower than seen in impeller mixed systems (Sucosky) while scaled.

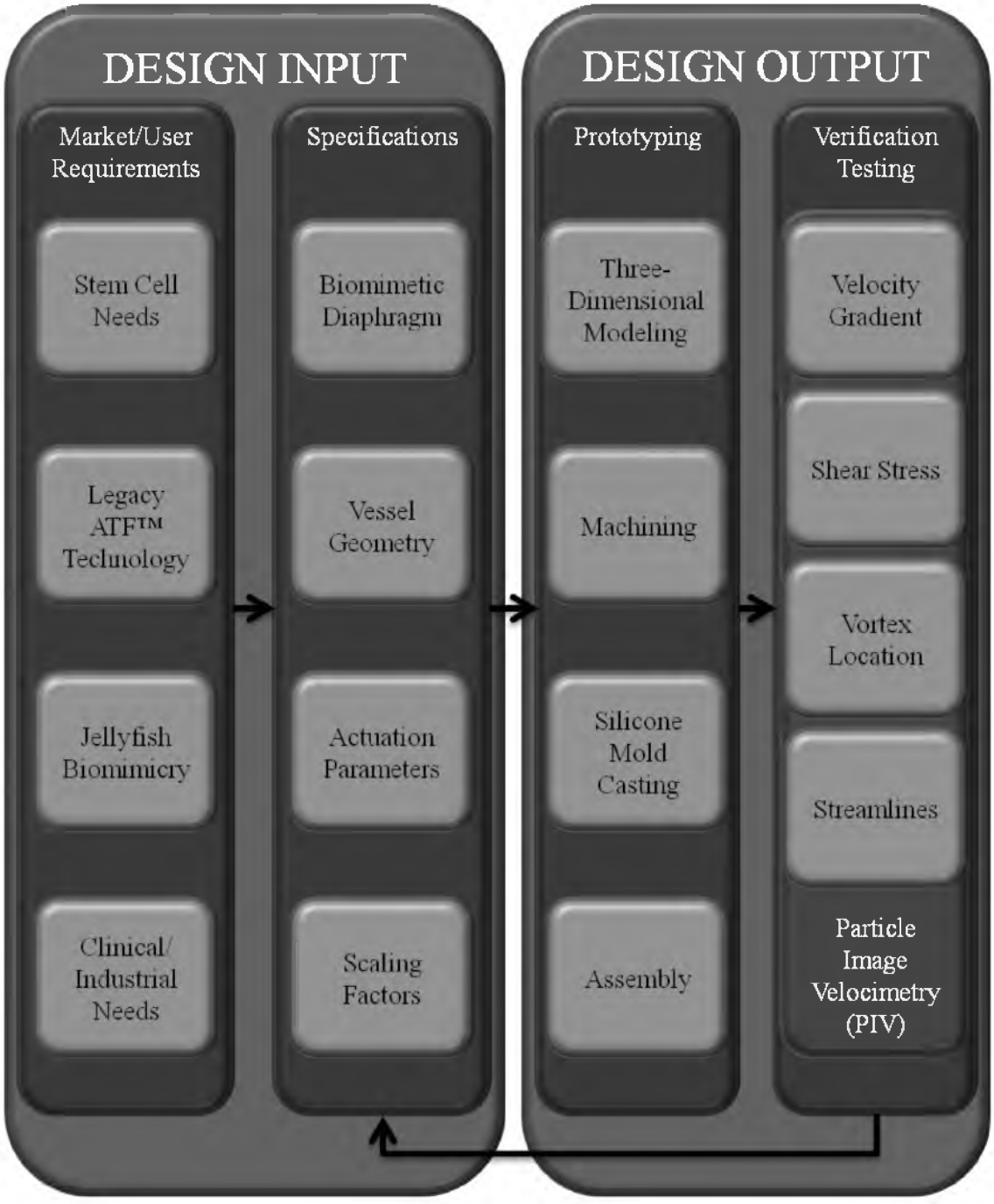

Figure 4.4 The design process consists of two primary phases, Design Input and Design Output. Requirements and Specifications were generated in Design Input which were then embodied in a testable prototype and verified through testing in Design Output.

REFERENCES

[1] F. M. Wurm, "Production of recombinant protein therapeutics in cultivated mammalian cells," *Nature Biotechnology*, vol. 22, no. 11, pp. 1393–1398, Nov. 2004.

[2] J. Kr, W. Kf, H. Ws, and Y. Mgs, "Recombinant protein therapeutics from CHO cells - 20 years and counting," *Chem. Eng. Prog.*, vol. 103, no. 10, pp. 40–47, 2007.

[3] "Biomanufacturing at overcapacity through to 2011," *in-PharmaTechnologist.com*. [Online] 2004, http://www.in-pharmatechnologist.com/Regulatory-Safety/Biomanufacturing-at-overcapacity-through-to-2011. (Accessed: 30-May-2012).

[4] I. Martin, D. Wendt, and M. Heberer, "The role of bioreactors in tissue engineering," *Trends Biotechnol.*, vol. 22, no. 2, pp. 80–86, Feb. 2004.

[5] S. Sharma, R. Raju, S. Sui, and W. Hu, "Stem cell culture engineering – process scale up and beyond," *Biotechnology Journal*, vol. 6, no. 11, pp. 1317–1329, Jul. 2011.

[6] R. Godoy-Silva, C. Berdugo, J. J. Chalmers, R. Godoy-Silva, C. Berdugo, and J. J. Chalmers, "Aeration, mixing, and hydrodynamics, animal cell bioreactors," in *Encyclopedia of Industrial Biotechnology: Bioprocess, Bioseparation, and Cell Technology*, Hoboken: John Wiley & Sons, Inc.

[7] T. Zhou, W. Zhou, W. Hu, J. Zhong, T.-C. Zhou, W.-W. Zhou, W. Hu, and J.-J. Zhong, "Bioreactors, cell culture, commercial production," in *Encyclopedia of Industrial Biotechnology: Bioprocess, Bioseparation, and Cell Technology*, Hoboken: John Wiley & Sons, Inc.

[8] J. E. Hambor, "Bioreactor design and bioprocess controls for industrialized cell processing," *BioProcess International*, vol. 10, no. 6, pp. 22–33, Jun. 2012.

[9] *Microcarrier Cell Culture Handbook*. GE Healthcare. Chalfont St. Giles, UK, 2005.

[10] A. W. Nienow, "Reactor engineering in large scale animal cell culture," *Cytotechnology*, vol. 50, no. 1–3, pp. 9–33, Mar. 2006.

[11] H. Zhang, W. Wang, C. Quan, and S. Fan, "Engineering considerations for process development in mammalian cell cultivation," *Current Pharmaceutical Biotechnology*, vol. 11, no. 1, pp. 103–112, 2010.

[12] S. S. Ozturk, "Engineering challenges in high density cell culture systems," *Cytotechnology*, vol. 22, no. 1, pp. 3–16, 1996.

[13] V. Restelli, M.-D. Wang, N. Huzel, M. Ethier, H. Perreault, and M. Butler, "The effect of dissolved oxygen on the production and the glycosylation profile of recombinant human erythropoietin produced from CHO cells," *Biotechnology and Bioengineering*, vol. 94, no. 3, pp. 481–494, 2006.

[14] R. Mirro and K. Voll, "Which impeller is right for your cell line? A guide to impeller selection for stirred-tank bioreactors," *BioProcess International*, vol. 7, no. 1, pp. 52–57, Jan. 2009.

[15] C. A. V. Rodrigues, T. G. Fernandes, M. M. Diogo, C. L. da Silva, and J. Cabral, "Stem cell cultivation in bioreactors," *Biotechnology Advances*, 2011.

[16] R. S. Cherry and E. T. Papoutsakis, "Physical mechanisms of cell damage in microcarrier cell culture bioreactors," *Biotechnology and bioengineering*, vol. 32, no. 8, pp. 1001–1014, 1988.

[17] A. Pollack, "A Stem-Cell-Based Drug Gets Approval in Canada," *The New York Times*, 17-May-2012.

[18] O. Lindvall, Z. Kokaia, and A. Martinez-Serrano, "Stem cell therapy for human neurodegenerative disorders - how to make it work," , *Published online: 01 July 2004; | doi:10.1038/nm1064*, vol. 10, pp. S42–S50, Jul. 2004.

[19] D. Jing, A. Parikh, J. M. Canty, and E. S. Tzanakakis, "Stem cells for heart cell therapies," *Tissue Engineering Part B: Reviews*, vol. 14, no. 4, pp. 393–406, Dec. 2008.

[20] L. T. Lock and E. S. Tzanakakis, "Stem/Progenitor cell sources of insulin-producing cells for the treatment of diabetes," *Tissue Engineering*, vol. 13, no. 7, pp. 1399–1412, Jul. 2007.

[21] B. G. Kim, D. H. Hwang, S. I. Lee, E. J. Kim, and S. U. Kim, "Stem cell-based cell therapy for spinal cord injury," *Cell Transplantation*, vol. 16, no. 4, pp. 355–364, 2007.

[22] L. Mazzini, K. Mareschi, I. Ferrero, E. Vassallo, G. Oliveri, N. Nasuelli, G. D. Oggioni, L. Testa, and F. Fagioli, "Stem cell treatment in amyotrophic lateral sclerosis," *Journal of the Neurological Sciences*, vol. 265, no. 1–2, pp. 78–83, Feb. 2008.

[23] B. O. Palsson and S. N. Bhatia, *Tissue Engineering*, 1st ed. Prentice Hall, 2003.

[24] R. Zweigerdt, "Large scale production of stem cells and their derivatives," *Adv. Biochem. Eng. Biotechnol.*, vol. 114, pp. 201–235, 2009.

[25] E. A. Ryan, J. R. T. Lakey, B. W. Paty, S. Imes, G. S. Korbutt, N. M. Kneteman, D. Bigam, R. V. Rajotte, and A. M. J. Shapiro, "Successful islet transplantation continued insulin reserve provides long-term glycemic control," *Diabetes*, vol. 51, no. 7, pp. 2148–2157, Jul. 2002.

[26] E. S. Tzanakakis, D. J. Hess, T. D. Sielaff, and W.-S. Hu, "Extracorporeal tissue engineered liver-assist devices," *Annual Review of Biomedical Engineering*, vol. 2, no. 1, pp. 607–632, 2000.

[27] J. T. Cormier, N. I. zur Nieden, D. E. Rancourt, and M. S. Kallos, "Expansion of undifferentiated murine embryonic stem cells as aggregates in suspension culture bioreactors," *Tissue Eng.*, vol. 12, no. 11, pp. 3233–3245, Nov. 2006.

[28] I. Sekiya, B. L. Larson, J. R. Smith, R. Pochampally, J. Cui, and D. J. Prockop, "Expansion of human adult stem cells from bone marrow stroma: Conditions that maximize the yields of early progenitors and evaluate their quality," *STEM CELLS*, vol. 20, no. 6, pp. 530–541, Nov. 2002.

[29] D. C. Colter, R. Class, C. M. DiGirolamo, and D. J. Prockop, "Rapid expansion of recycling stem cells in cultures of plastic-adherent cells from human bone marrow," *PNAS*, vol. 97, no. 7, pp. 3213–3218, Mar. 2000.

[30] N. Kotobuki, M. Hirose, Y. Takakura, and H. Ohgushi, "Cultured autologous human cells for hard tissue regeneration: Preparation and characterization of mesenchymal stem cells from bone marrow," *Artificial Organs*, vol. 28, no. 1, pp. 33–39, Jan. 2004.

[31] M. F. Pittenger, "Multilineage potential of adult human mesenchymal stem cells," *Science*, vol. 284, no. 5411, pp. 143–147, Apr. 1999.

[32] A. J. Nauta and W. E. Fibbe, "Immunomodulatory properties of mesenchymal stromal cells," *Blood*, vol. 110, no. 10, pp. 3499–3506, Nov. 2007.

[33] L. Sensebé, M. Krampera, H. Schrezenmeier, P. Bourin, and R. Giordano, "Mesenchymal stem cells for clinical application," *Vox Sang.*, vol. 98, no. 2, pp. 93–107, Feb. 2010.

[34] L. Fouillard, A. Chapel, D. Bories, S. Bouchet, J.-M. Costa, H. Rouard, P. Hervé, P. Gourmelon, D. Thierry, M. Lopez, and N. C. Gorin, "Infusion of allogeneic-related HLA mismatched mesenchymal stem cells for the treatment of incomplete engraftment following autologous haematopoietic stem cell transplantation," *Leukemia*, vol. 21, no. 3, pp. 568–570, Jan. 2007.

[35] K. Le Blanc and O. Ringdén, "Immunobiology of human mesenchymal stem cells and future use in hematopoietic stem cell transplantation," *Biology of Blood and Marrow Transplantation*, vol. 11, no. 5, pp. 321–334, May 2005.

[36] A. Leri, J. Kajstura, P. Anversa, and W. H. Frishman, "Myocardial regeneration and stem cell repair," *Current Problems in Cardiology*, vol. 33, no. 3, pp. 91–153, Mar. 2008.

[37] J. R. Sanchez-Ramos, "Neural cells derived from adult bone marrow and umbilical cord blood," *Journal of Neuroscience Research*, vol. 69, no. 6, pp. 880–893, Aug. 2002.

[38] S. Wakitani, K. Imoto, T. Yamamoto, M. Saito, N. Murata, and M. Yoneda, "Human autologous culture expanded bone marrow mesenchymal cell transplantation for repair of cartilage defects in osteoarthritic knees," *Osteoarthritis and Cartilage*, vol. 10, no. 3, pp. 199–206, Mar. 2002.

[39] A. I. Caplan, "The mesengenic process," *Clin Plast Surg*, vol. 21, no. 3, pp. 429–435, Jul. 1994.

[40] D. Brindley, K. Moorthy, J.-H. Lee, C. Mason, H.-W. Kim, and I. Wall, "Bioprocess forces and their impact on cell behavior: Implications for bone regeneration therapy," *Journal of Tissue Engineering*, Oct. 2011.

[41] M. A. Kinney, C. Y. Sargent, and T. C. McDevitt, "The multiparametric effects of hydrodynamic environments on stem cell culture," *Tissue Eng Part B Rev*, vol. 17, no. 4, pp. 249–262, Aug. 2011.

[42] K. Ksiazek, "A comprehensive review on mesenchymal stem cell growth and senescence," *Rejuvenation Res*, vol. 12, no. 2, pp. 105–116, Apr. 2009.

[43] C. Fehrer, R. Brunauer, G. Laschober, H. Unterluggauer, S. Reitinger, F. Kloss, C. Gülly, R. Gaßner, and G. Lepperdinger, "Reduced oxygen tension attenuates differentiation capacity of human mesenchymal stem cells and prolongs their lifespan," *Aging Cell*, vol. 6, no. 6, pp. 745–757, Aug. 2007.

[44] F. dos Santos, P. Z. Andrade, J. S. Boura, M. M. Abecasis, C. L. da Silva, and J. Cabral, "Ex vivo expansion of human mesenchymal stem cells: a more effective cell proliferation kinetics and metabolism under hypoxia," *Journal of Cellular Physiology*, vol. 223, no. 1, pp. 27–35, 2010.

[45] M. Grolms, R. Olmer, U. Martin, and R. Zweigerdt, "Facilitating scale up: controlled stem cell cultivation in stirred suspension bioreactors," *BioProcess International*, pp. 19–21, May 2011.

[46] P. Godara, C. D. McFarland, and R. E. Nordon, "Design of bioreactors for mesenchymal stem cell tissue engineering," *Journal of Chemical Technology and Biotechnology*, vol. 83, no. 4, pp. 408–420, Apr. 2008.

[47] F. Zhao, R. Chella, and T. Ma, "Effects of shear stress on 3-D human mesenchymal stem cell construct development in a perfusion bioreactor system: Experiments and hydrodynamic modeling," *Biotechnol. Bioeng.*, vol. 96, no. 3, pp. 584–595, Feb. 2007.

[48] J. A. Rowley, "Developing cell therapy biomanufacturing processes," *Chemical Engineering Progress*, vol. 106, no. 11, pp. 50–55, Nov. 2010.

[49] F. Ulloa-Montoya, C. M. Verfaillie, and W.-S. Hu, "Culture systems for pluripotent stem cells," *Journal of Bioscience and Bioengineering*, vol. 100, no. 1, pp. 12–27, Jul. 2005.

[50] G. Eibes, F. dos Santos, P. Z. Andrade, J. S. Boura, M. M. A. Abecasis, C. L. da Silva, and J. M. S. Cabral, "Maximizing the ex vivo expansion of human mesenchymal stem cells using a microcarrier-based stirred culture system," *Journal of Biotechnology*, vol. 146, no. 4, pp. 194–197, Apr. 2010.

[51] C. J. Hewitt, K. Lee, A. W. Nienow, R. J. Thomas, M. Smith, and C. R. Thomas, "Expansion of human mesenchymal stem cells on microcarriers," *Biotechnology Letters*, vol. 33, no. 11, pp. 2325–2335, Jul. 2011.

[52] Q.-F. Wu, C.-T. Wu, B. Dong, and L.-S. Wang, "Cultivation of human mesenchymal stem cells on macroporous CultiSpher G microcarriers," *Zhongguo Shi Yan Xue Ye Xue Za Zhi*, vol. 11, no. 1, pp. 15–21, Feb. 2003.

[53] C. M. Begley and S. J. Kleis, "The fluid dynamic and shear environment in the NASA/JSC rotating-wall perfused-vessel bioreactor," *Biotechnol. Bioeng.*, vol. 70, no. 1, pp. 32–40, Oct. 2000.

[54] T. G. Hammond and J. M. Hammond, "Optimized suspension culture: The rotating-wall vessel," *Am J Physiol Renal Physiol*, vol. 281, no. 1, pp. F12–F25, Jul. 2001.

[55] S. M. Azarin and S. P. Palecek, "Development of scalable culture systems for human embryonic stem cells," *Biochemical Engineering Journal*, vol. 48, no. 3, pp. 378–384, 2010.

[56] "BioProcess International Announces Winners of the 2012 BioProcess International Awards." [Online]. Available: http://www.prweb.com/releases/2012/10/prweb9992586.htm. [Accessed: 01-Dec-2012].

[57] J. O. Dabiri, "Flow patterns generated by oblate medusan jellyfish: Field measurements and laboratory analyses," *Journal of Experimental Biology*, vol. 208, no. 7, pp. 1257–1265, Apr. 2005.

[58] J. C. Nawroth, H. Lee, A. W. Feinberg, C. M. Ripplinger, M. L. McCain, A. Grosberg, J. O. Dabiri, and K. K. Parker, "A tissue-engineered jellyfish with biomimetic propulsion," *Nature Biotechnology*, vol. 30, no. 8, pp. 792–797, 2012.

[59] J. O. Dabiri, "Optimal vortex formation as a unifying principle in biological propulsion," *Annual Review of Fluid Mechanics*, vol. 41, pp. 17–33, 2009.

[60] S. C. Shadden, K. Katija, M. Rosenfeld, J. E. Marsden, and J. O. Dabiri, "Transport and stirring induced by vortex formation," *Journal of Fluid Mechanics*, vol. 593, Nov. 2007.

[61] K. Katija and J. O. Dabiri, "A viscosity-enhanced mechanism for biogenic ocean mixing," *Nature*, vol. 460, no. 7255, pp. 624–626, Jul. 2009.

[62] S. P. Colin, J. H. Costello, J. O. Dabiri, A. Villanueva, J. B. Blottman, B. J. Gemmell, and S. Priya, "Biomimetic and live medusae reveal the mechanistic advantages of a flexible bell margin," *PLoS ONE*, vol. 7, no. 11, p. e48909, 2012.

[63] J. Comley, "3D Cell Culture - Easier said than done.pdf," *Drug Discovery World*, pp. 25–41, Summer-2010.

[64] P. Sucosky, D. F. Osorio, J. B. Brown, and G. P. Neitzel, "Fluid mechanics of a spinner-flask bioreactor," *Biotechnology and Bioengineering*, vol. 85, no. 1, pp. 34–46, Jan. 2004.

[65] R. J. Adrian, "Particle-imaging techniques for experimental fluid mechanics," *Annual Review of Fluid Mechanics*, vol. 23, no. 1, pp. 261–304, 1991.

[66] C. E. Willert and M. Gharib, "Digital particle image velocimetry," *Experiments in Fluids*, vol. 10, no. 4, pp. 181–193, Jan. 1991.

[67] J. Westerweel, "Fundamentals of digital particle image velocimetry," *Measurement Science and Technology*, vol. 8, no. 12, pp. 1379–1392, Dec. 1997.

[68] J. Schindelin, I. Arganda-Carreras, E. Frise, V. Kaynig, M. Longair, T. Pietzsch, S. Preibisch, C. Rueden, S. Saalfeld, B. Schmid, J.-Y. Tinevez, D. J. White, V. Hartenstein, K. Eliceiri, P. Tomancak, and A. Cardona, "Fiji: An open-source platform for biological-image analysis," *Nature Methods*, vol. 9, no. 7, pp. 676–682, Jun. 2012.

[69] I. Arganda-Carreras, C. Sorzano, R. Marabini, J. Carazo, C. Ortiz-de-Solorzano, and J. Kybic, "Consistent and elastic registration of histological sections using vector-spline regularization," *Computer Vision Approaches to Medical Image Analysis*, pp. 85–95, 2006.

[70] W. Thielicke and E. J. Stamhuis, "PIVlab update 1.32," *PIVlab - Time-Resolved Digital Particle Image Velocimetry Tool for MATLAB*. 25-Sep-2012.

[71] P. Sucosky, "Flow Characterization and modeling of cartilage development in a spinner-flask bioreactor", Ph.D. dissertation, Mech. Eng., Georgia Institute of Technology, 2005.